



INSTITUT DE FRANCE
Académie des sciences

Comptes Rendus

Chimie

Dominique Bazin, Elise Boudierlique, Michel Daudon, Vincent Frochot, Jean-Philippe Haymann, Emmanuel Letavernier, Frederik Tielens and Raphaël Weil

Scanning electron microscopy—a powerful imaging technique for the clinician


Volume 25, Special Issue S1 (2022), p. 37-60

Published online: 9 August 2021

<https://doi.org/10.5802/crchim.101>

Part of Special Issue: Microcrystalline pathologies: Clinical issues and nanochemistry

Guest editors: Dominique Bazin (Université Paris-Saclay, CNRS, ICP, France), Michel Daudon, Vincent Frochot, Emmanuel Letavernier and Jean-Philippe Haymann (Sorbonne Université, INSERM, AP-HP, Hôpital Tenon, France)

 This article is licensed under the
CREATIVE COMMONS ATTRIBUTION 4.0 INTERNATIONAL LICENSE.
<http://creativecommons.org/licenses/by/4.0/>



Les Comptes Rendus. Chimie sont membres du
Centre Mersenne pour l'édition scientifique ouverte
www.centre-mersenne.org
e-ISSN : 1878-1543



Microcrystalline pathologies: Clinical issues and nanochemistry / *Pathologies microcristallines : questions cliniques et nanochimie*

Scanning electron microscopy—a powerful imaging technique for the clinician

Dominique Bazin^{*, a, b}, Elise Boudierlique^{c, d, e}, Michel Daudon^{c, d, e},
Vincent Frochot^{c, d, e}, Jean-Philippe Haymann^{c, d, e}, Emmanuel Letavernier^{c, d, e},
Frederik Tielens^f and Raphaël Weil^a

^a Institut de Chimie Physique, UMR CNRS 8000, Bâtiment 350, Université Paris Saclay, 91405 Orsay cedex, France

^b Laboratoire de physique des solides, UMR CNRS 8502, Bâtiment 510, Université Paris-Sud, 91405 Orsay cedex, France

^c Sorbonne Universités, UPMC Univ Paris 06, UMR S 702, Paris, France

^d INSERM, UMR S 702, Paris, France

^e Explorations fonctionnelles multidisciplinaires, AP-HP, Hôpital Tenon, Paris, France

^f General Chemistry (ALGC), Vrije Universiteit Brussel (Free University Brussels-VUB), Pleinlaan 2, 1050 Brussel, Belgium

E-mails: dominique.bazin@universite-paris-saclay.fr (D. Bazin), Eliseboud@aol.com (E. Boudierlique), michel.daudon@aphp.fr (M. Daudon), vincent.frochot@aphp.fr (V. Frochot), jean-Philippe.haymann@aphp.fr (J.-P. Haymann), emmanuel.letavernier@aphp.fr (E. Letavernier), frederik.tielens@vub.be (E. Tielens), raphael.weil@u-psud.fr (R. Weil)

Abstract. Since its first use several decades ago, scanning electron microscopy has been used in numerous investigations dedicated to biological systems. This contribution focuses on observations on pathological calcifications in order to review several major applications of primary importance to the clinician. Among these, we highlight such observations as medical diagnostic tools in pathologies arising from primary hyperoxaluria and urinary infections.

Keywords. Scanning electron microscopy, Pathological calcifications, Kidney stones, Breast calcifications, Breast cancer.

Published online: 9 August 2021

1. Introduction

The history of the electron microscope dates back to the first third of the twentieth century when E. Ruska

and M. Knoll, from the University of Berlin, created the first instrument in 1931 [1,2]. Basically, scanning electron microscopy (SEM) uses a finely focused beam of electrons in order to produce a resolution image of a sample [3]. In the case of biological samples, such an experimental setup allows imaging with a lateral resolution around 200 nm

* Corresponding author.

without sample preparation (magnification around 45,000).

Several investigations of structures related to kidney stones (KS) were performed as early as over 40 years ago [4–9]. Fujita *et al.* [5] showed that SEM precisely describes the three-dimensional architecture of the endothelial cell. As far as KS are concerned, Phaneuf-Mimeault and Tawashi [6] showed that the surface crystals have random axial orientations and that the gross configuration seems to be determined by the fibrous organic matrix.

Nowadays, SEM of pathological calcifications [10–12] is a very active research field. Typical recent publications include studies on kidney [13–24], salivary stones [25], breast [26–28], cardiovascular system [29, 30], cartilage [31,32], gallstones [33], prostatic stones [34,35], thyroid [36], liver [37], ileal [38], or medical devices [39]. These examples convincingly show that SEM is an essential laboratory tool that continues to provide new clues about the pathogenesis of these biological samples.

This success may be ascribed to the significant recent advances in the various components of a scanning electron microscope, namely the electron gun, optics, and detectors, enabling entirely new opportunities [3,40]. For instance, detection at low voltage (between 0.5 and 2 kV) without the usual surface carbon deposition leads to novel breakthroughs regarding pathological calcifications [41,42] as well as tissue alterations [43,44]. Additionally, biological samples used for nanometer scale observations are compatible with other techniques such as Fourier Transform Infra-Red (FTIR), Raman, and Nano-UV spectroscopies [45,46].

The aim of this survey is to use selected examples to illustrate different research applications of SEM. We show that a precise description of crystallite morphology and surface may be a basis for diagnosis or deciphering the biomechanism governing the genesis of concretions and ectopic calcifications [47,48]. We define “nanocrystals” and “crystallites” according to Van Meerssche and Feneau-Dupont, i.e., crystallites (measuring typically some tens of micrometers) are made of a collection of nanocrystals (measuring typically some hundreds of nanometers), to describe the structural hierarchy of pathological calcifications [49]. We will start by briefly recapitulating the underlying physics of SEM.

2. Basic SEM physics

The first component of a SEM is the electron gun [50]. Conventional electron guns use thermal energy to emit electrons from a cathode. The main disadvantage of this experimental device is related to the surface area of the source which emits electrons. Its dimension is rather large (10–30 μm) and the energy spread spans a few electron volts, because of the excess thermal energy supplied by heating. A new type of electron gun was developed in the late twentieth century. It is based on the tunneling, or Schottky effect, to produce electrons from a tip, in which case the source size is less than 10 nm, and the energy dispersion is now only a few tenths of an electron volt.

The second key element defining the properties of the SEM is constituted by a set of detectors. These depend on the fact that the electron beam focused over a surface (Figure 1) produces various kinds of electrons as well as photons [3], allowing the experimentalist to gather information regarding the surface topography and the elemental composition of the sample at the submicrometer scale [51].

Among these components, a backscatter electron detector (BSD) detects elastically scattered electrons, and takes advantages of the fact that higher atomic number atoms have a higher probability of producing an elastic collision because of their greater cross-sectional area [52]. Thus, brightness of the image obtained is directly proportional to atomic number, so backscatter electron (BSE) images provide an elegant way to distinguish different chemical phases at the sample surface. BSE detectors are typically located above the sample in the sample chamber.

The so called secondary electrons [53] are lower energy electrons emitted when a solid is irradiated with high energy electrons or other particles; two kinds of detectors, namely the conventional Everhart–Thornley type and in-lens detectors, are usually positioned in the sample chamber. The former produces images which are more dependent on the sample topography than the ones obtained by a BSE detector.

One of the key advantages of modern SEM instruments is their spatial resolution [51–54]. By using electrons instead of photons for imaging samples, SEM can achieve nanometer spatial resolution [55–57]. This ability depends on several factors such

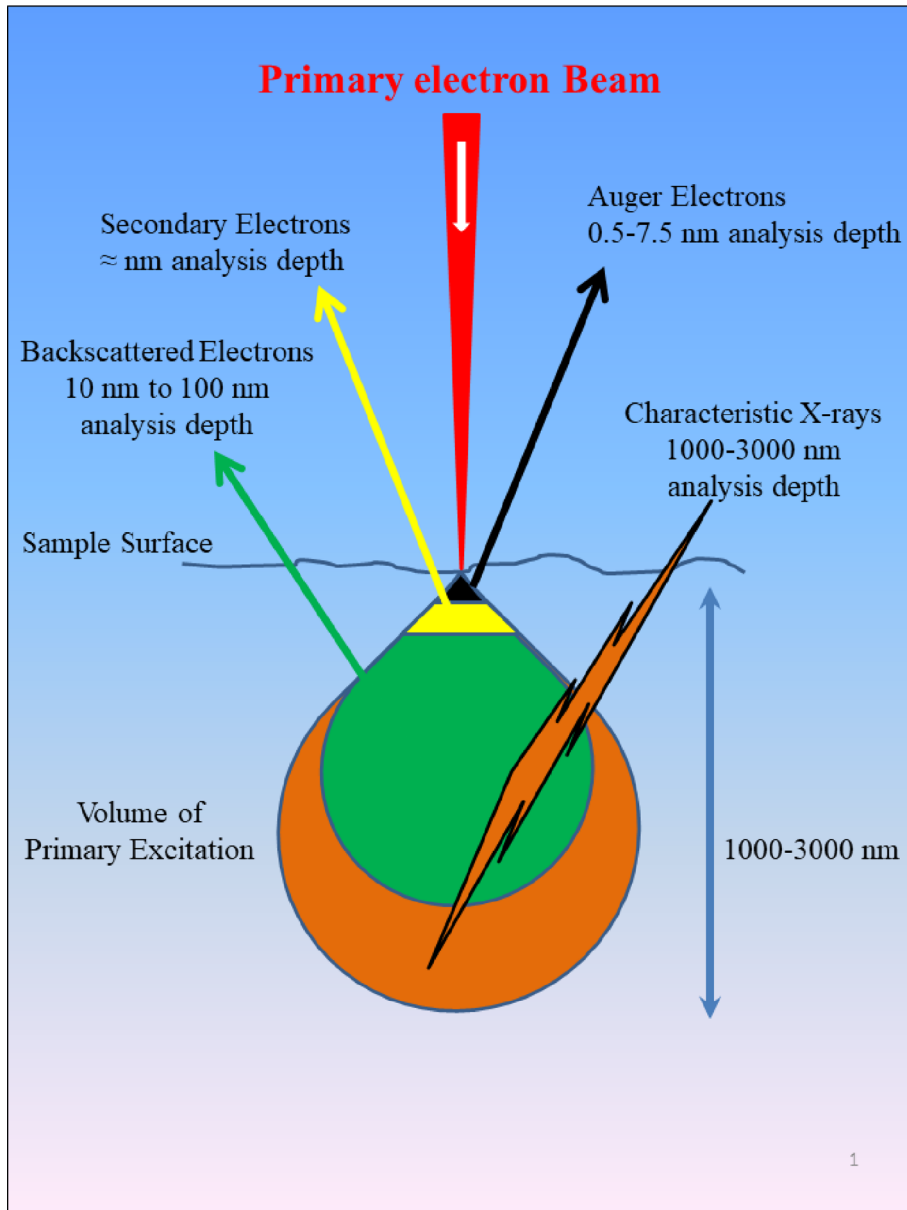


Figure 1. Schematic representation of the different kinds of particles i.e., electrons (backscattered electrons, secondary electrons, Auger electrons) and photons produced after the irradiation of matter by primary electrons. The analysis depth is given for the different particles.

as the electron spot size, which is determined by the way electrons are produced and focused, as well as the interaction volume of the electron beam with the sample. Even though they fall short of providing atomic resolution, some SEMs can typically achieve

resolution between 1 and 20 nm. The distance from the final pole piece of the lens to the sample, called working distance, is about a few millimeters. To improve the resolution, working distance, source energy, and current density are crucial parameters.

3. Sample preparation

Visualizing biological samples with an electron microscope is not easy, mostly because of the intrinsic nature of the electron and matter interactions which defined the image formation. In order to be able to collect SEM images, biological samples have to be placed inside high vacuum. Such experimental conditions usually lead to a quite complex preparation protocol [58–60].

In the case of pathological calcifications, it is of primary importance to preserve the physicochemical integrity of the abnormal deposit. Such priority is associated to the relationship which exists between the physicochemistry of the calcification (i.e., the chemical composition and the crystal morphology) and the pathology which induced its formation [61–64]. In the case of KS, there is simply no preparation. The concretions are directly positioned under the electron beam. In our case, a field-effect “gun” microscope, namely a Zeiss SUPRA55-VP SEM, was used for the observation of microstructure. High-resolution observations were obtained by an Everhart–Thornley SE detector. To maintain the physicochemical integrity of the samples, measurements were taken without the usual deposits of carbon at the surface of the sample (Figure 2).

Regarding tissue embedded in paraffin, three to five micron slices are deposited on low-e microscope slides (MirrIR, Kevley Technologies, Tienta Sciences, Indianapolis). The paraffin was then chemically removed (xylene 100% during 30 min to 4 h) in order to improve the crystal detection under the microscope (Figure 2).

4. Crystal morphology

It is now well accepted that a relationship exists between crystallographic structure and morphology, exemplified by Jean Baptiste Louis Romé de l’Isle’s discovery of the fact that the various shapes of crystals of the same natural or artificial substance are all intimately related to each other. More precisely, by measuring the angles between the faces of crystals, he established the fundamental principle that these angles are characteristic for a given substance. This discovery is known as the law of constant angles [65].

A second important relationship, the law of symmetry, established by Haiüy [66], states that the edges,

angles, and faces of a crystal form are related by symmetry. Thus, for example, when one face of an octahedron is modified by its combination with another form (for example by truncation), all other faces of the octahedron should be modified at this point in the same way.

In fact, according to the Gibbs–Curie–Wulff theorem [67], the equilibrium crystal form will be such as to minimize the total surface energy for a given volume. This equilibrium form is defined in vacuum. Unfortunately, the presence of other compounds can modify this equilibrium through adsorption processes. As recalled by Zhang [68], the shape of a crystal is governed by the relative growth rates of each of the crystal faces present. The most prominent face of a crystal is the slowest growing, while the smallest face is the fastest growing [69]. The interplay between thermodynamics and kinetics during the growth process makes predictions of the final geometry challenging [70].

5. SEM as diagnostic tool

Some authors have suggested SEM as a fundamental method for routine urinary stone identification, which also reveals additional detailed information unobtainable by other methods, such as the morphology, the size, and the elemental composition of crystallites present in kidney stones [18]. At this point, recall that more than one hundred chemical phases have been identified in kidney stones and more than 100 different etiologies may be involved in stone formation [61–64]. Moreover, some chemical phases, such as whewellite ($\text{CaC}_2\text{O}_4 \cdot \text{H}_2\text{O}$) or weddellite ($\text{CaC}_2\text{O}_4 \cdot 2 \cdot x\text{H}_2\text{O}$ (with $x = 0-0.5$) [71] may correspond to very different morphologies. According to the morphoconstitutional model [61–64,72], five different morphological aspects of whewellite stones, namely Ia, Ib, Ic, Id, and Ie, correspond to five different lithogenic conditions. Also, phase transformations such as the transition of weddellite to whewellite (for the oxalates) or brushite to apatite (for the phosphates) occur (Figure 3). Finally, it is not possible to evaluate the carbonation rate of apatite, an essential parameter related to infection [73], through SEM. Thus, due to this diversity of chemical phases, crystal morphology within a single chemical phase, as well as the possibility of phase transitions,

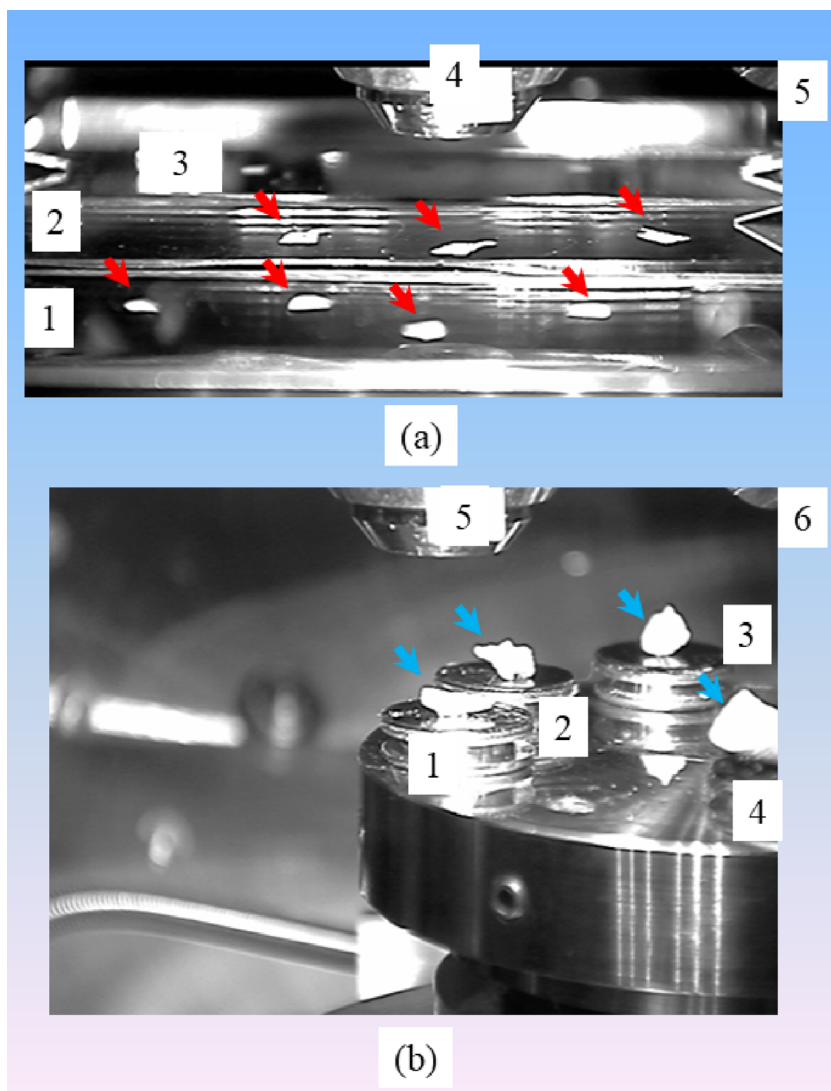


Figure 2. (a) Skin biopsies (red arrows) positioned on low-e microscope slides (1, 2, 3) (MirrIR, Kevley Technologies, Tienta Sciences, Indianapolis) compatible with Fourier transform Infrared Spectroscopy, an electron gun (4), an Everhart–Thornley SE detector (5). (b) Kidney stones (blue arrows) on their support (1 to 4), an electron gun (5), an Everhart–Thornley SE detector (6).

SEM cannot replace the gold standard FTIR spectroscopy [74–76].

Nevertheless, there are numerous exceptions where SEM provides detailed information at the micrometer scale, which can be of primary importance for the clinician (Figure 4).

For example, in the case of primary hyperoxaluria, the most severe lithogenetic disease, we have shown that the morphology of whewellite crystallites is dis-

tinctive (Figures 4a and b) from that observed in the case of dietary hyperoxaluria. Such direct examination constitutes a simple, rapid, and inexpensive tool that would suggest early diagnosis of primary hyperoxaluria type 1 [41,42]. Recall that multiple defective genes can underlie this disease so the genetic approach to diagnosis can be long and expensive. For calcium oxalate dihydrate, it has been established that the presence of dodecahedral crystallites

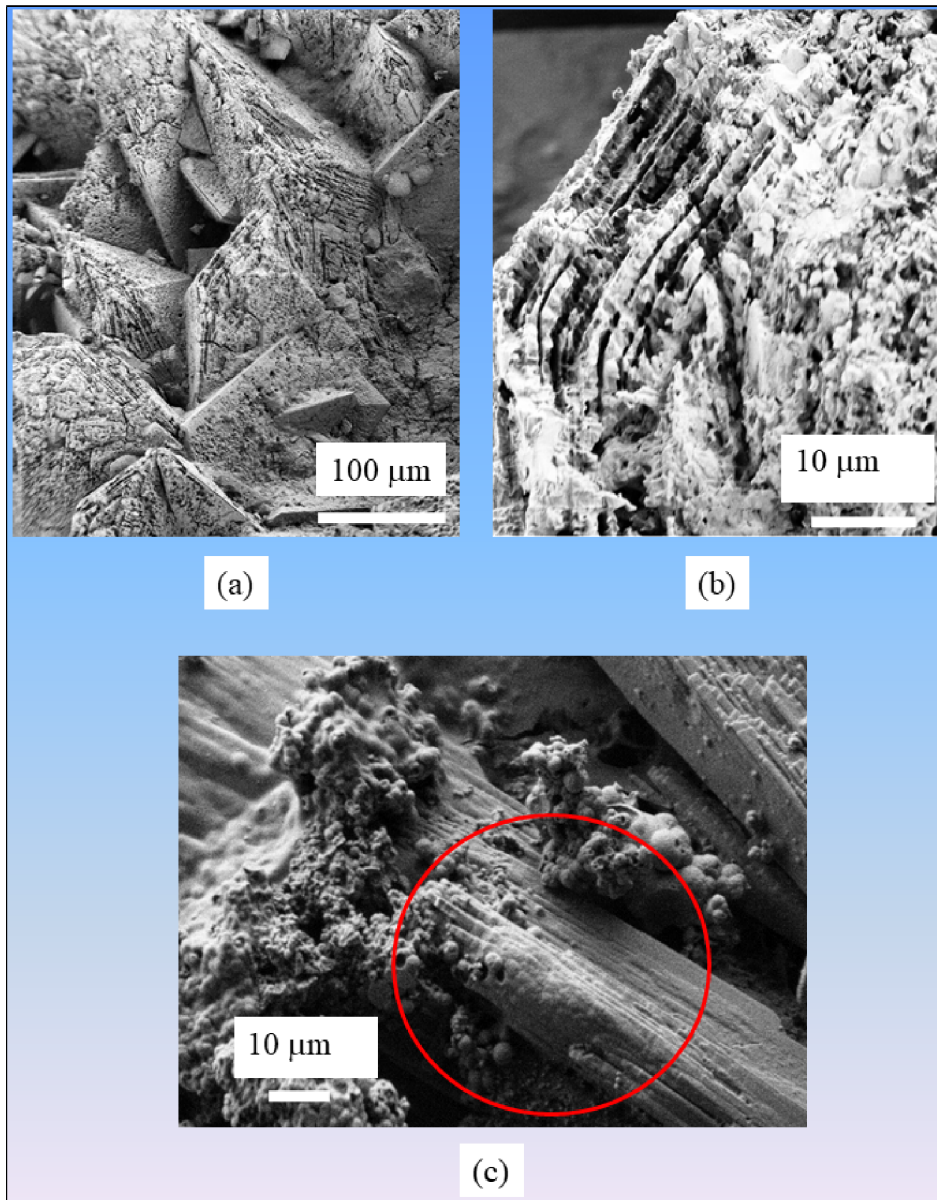


Figure 3. (a) SEM observation showing weddellite crystallites displaying their usual bipyramidal morphologies with alteration at their surface induced by a phase transition. (b) SEM observations showing the transition between acicular brushite and spherical apatite.

(i.e., bipyramidal with a thick zone between the two pyramids) is indicative of heavy hypercalciuria [77].

Another case where SEM makes a crucial contribution concerns kidney stones related to infection (Figure 4c). In patients with kidney stones without struvite, and with negative urine culture results, we have proposed SEM observations in order to confirm

the possible presence of bacterial imprints [73,78]. Of note, due to the crystal size such bacterial imprints cannot be detected in struvite, except in the areas of the stone that contain apatite crystals.

Regarding the quantitative aspect, such approach occurs in the case of crystalluria when the number of crystallites is considered [77], but it is difficult to

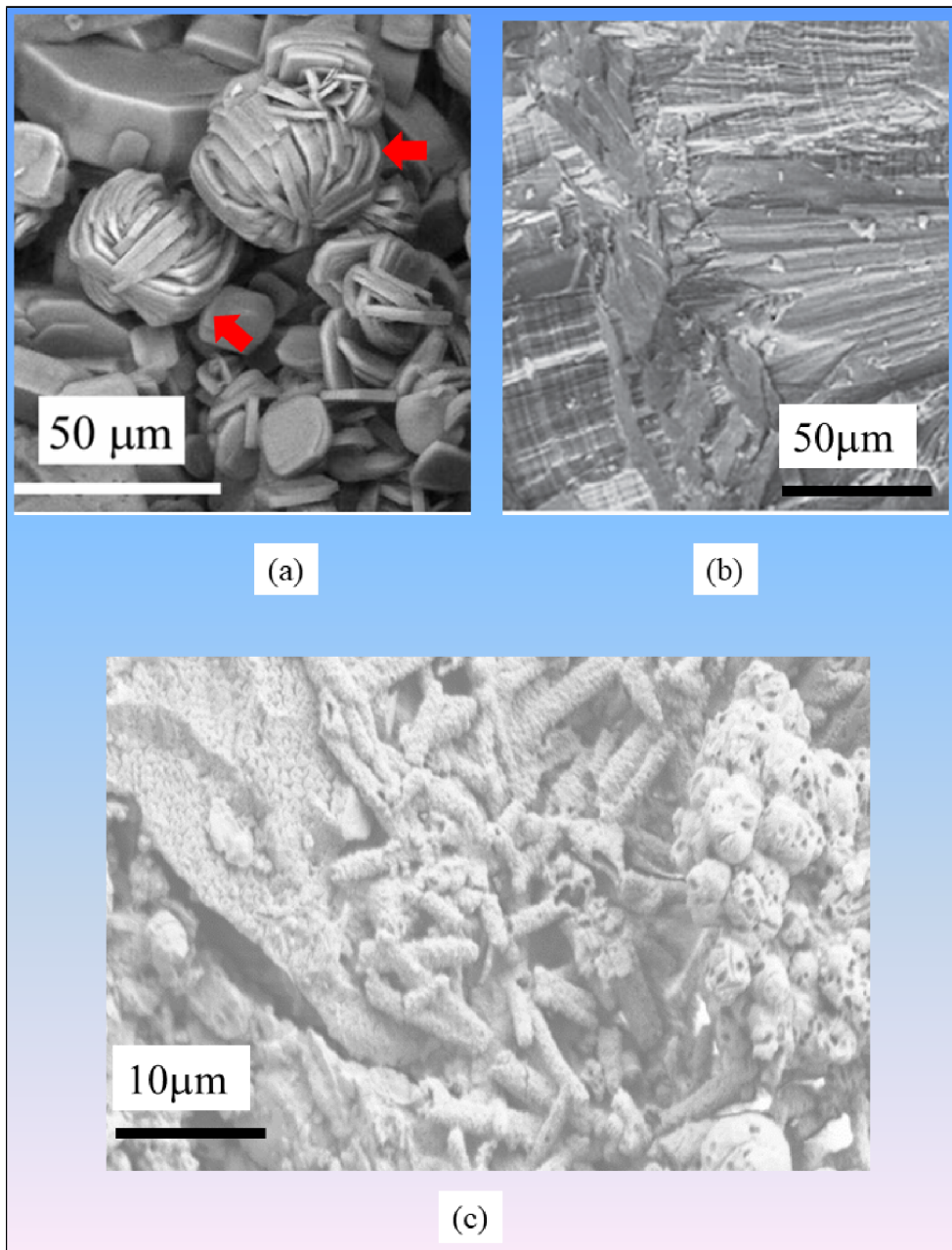


Figure 4. SEM observation of a kidney stone related to (a) genetic primary hyperoxaluria and (b) related to intermittent hyperoxaluria of dietary origin. (c) SEM observation of bacterial imprints and bacteria surrounded by calcifications.

have a similar approach in the case of SEM observations. In the case of kidney stones, only the surface is examined and a significant quantitative determination of the number of crystallites per unit sur-

face needs numerous observations. From a clinical practice point of view, FTIR spectroscopy constitutes a cheaper and quicker method to obtain a quantitative information regarding the chemical composition

[69–71]. Nevertheless, in the near future, such determination through SEM observations of the surface of the kidney stone may be relevant with the help of machine learning [79].

6. Elucidating the pathogenesis of Randall's plaque

Randall's plaque represents a major issue in urology [80,81]. Several papers report evidence that Randall's plaque (RP) present at the tip of the renal papilla may initiate whewellite (Figure 5a) and more rarely weddellite stones [82–91]. Some of these investigations have been dedicated to the pathogenesis of this pathological calcification; recent data show clearly that vitamin D and calcium supplementation accelerates the formation of RP in a murine model [91].

Other publications report various RP chemical compositions. While calcium phosphate apatite (CA) as well as amorphous carbonated calcium phosphate (ACCP) are the major components of most RPs (Figure 5b) [92], other chemical phases such as whitlockite, brushite, and sodium hydrogen urate monohydrate (NaUr) [90] have been identified in about 5% of RP (Figure 5c). Such chemical diversity underlines the fact that several very different mechanisms may be related to the pathogenesis of RP.

Note that RP constituted by NaUr appeared to be sex dependent. NaUr-containing RP was found in 4.3% of stones from male patients and in only 0.6% of cases in female patients ($p < 0.00001$). This is consistent with the ratio observed in stones made of NaUr as the major component. Moreover, RP also exists on weddellite KS (Figure 5d), although the fact that weddellite crystals are very large may explain why RP is observed preferentially on whewellite KS.

A striking feature of RP composed of CA is related to their structure. As we can see in Figure 6, all the RP present on whewellite KS show the same morphology [93,94]. RP are made of a conglomeration of calcified tubules and vessels (vasa recta) reflecting the morphology of the tip of the papilla. Figure 6e shows a normal papilla where we can see the tubule exit orifices (yellow arrows).

Higher magnification observations are shown in Figure 7. Note the calcium phosphate cluster within one tubular lumen (Figure 7a, yellow arrow), while other tubules are empty with calcified walls (black arrow). Figure 7b shows that the walls of the tubules

are constituted by an agglomeration of CA spheres [95–97]. Finally, in Figure 7c, a plug inside the tubule is visualized [98].

7. The process of kidney stone growth from RP

We now discuss the growth of a whewellite KS from RP. Only a few papers discuss this particular point [93,94,99,100]. According to Sethmann *et al.* [94], ions from CaP-supersaturated interstitial fluid may diffuse through porous RP into the urine, where a resulting local increase in whewellite supersaturation could trigger crystal nucleation and hence initiate stone formation (Figure 8).

At this point, we must emphasize that calcium oxalate crystallites are present in urine even in the case of healthy subjects (7% vs. 40% in stone formers) [101]. It is their high occurrence over time which is abnormal. In fact, in our case, we observe “classical” whewellite crystallites (Figure 6). Note that in some cases we found whewellite crystallites coated with calcium phosphate as well, which can be due to simple deposition of urinary calcium phosphate. In the pathogenesis model we have proposed, large randomly oriented whewellite crystals are trapped on a phase of CA crystals embedded in proteins acting as a “glue” [93]. This conjecture is clearly supported by Figure 8c. Thus, it seems that the hypothesis of epitaxy between Ca phosphate (RP) and Ca oxalate (KS) is not relevant in this case [100]. Note also that the surface of biological apatite is hydrated [102–104].

The surfaces exposed by the whewellite crystallites are those of the growing crystal in aqueous conditions. The crystal description can be found in our recent paper [70]. We can see (Figure 7) the (100), (12-1), and (010) surface of the crystallites, showing the different (12-1)/(010) surface ratios due to the growth process.

Theoretically some attempts have been performed to predict and understand oxalate polymorphism in the past [70,105]. A very pedagogical paper on the topic has been written by Millan [105]. Since that time the chemical computational tools have been evolved dramatically and we recently revisited this topic using quantum chemical DFT methods and molecular dynamic tools. Note that DFT offers the opportunity to assess adsorption of molecules and thus the reactivity as well as the morphology of small crystals [106–108].

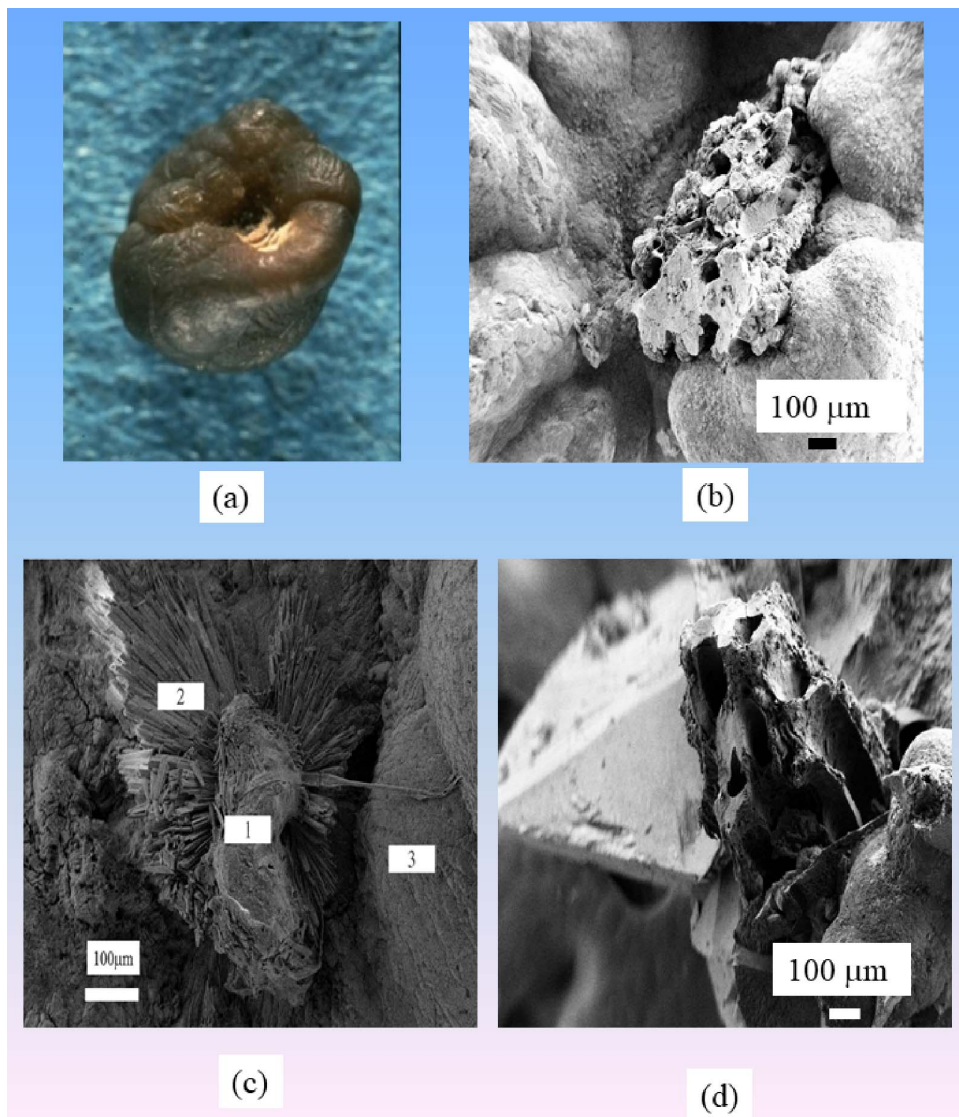


Figure 5. (a) RP made of CA positioned on a whewellite KS. (b) SEM observation of an RP made of CA. (c) SEM observation of an RP made of NaUr. Microscopic aspect of an RP (areas 1 and 2) composed of a mixture of NaUr needles and carapatite attached to a whewellite calculus (area 3). NaUr needles of large dimension are visible on area 2. (d) RP on a weddellite KS. Note the large size of weddellite crystallites, which may explain why RP is rarely observed on weddellite stones.

In 2001, Millan [105] suggested carefully that, in his conclusion, not only the thermodynamics play a role in the expressed morphology but also the kinetics of the formation of the different surfaces. This result was clearly confirmed by us recently [70]. Moreover, we showed that the effect on the surface for-

mation kinetics can be expressed by including a correction factor to the surface energies. This correction factor, which is purely mathematical, is expected to be related with the kinetics and can be related to the reactions taking place in a DFT-Molecular dynamics calculation on the growth of a specific sur-

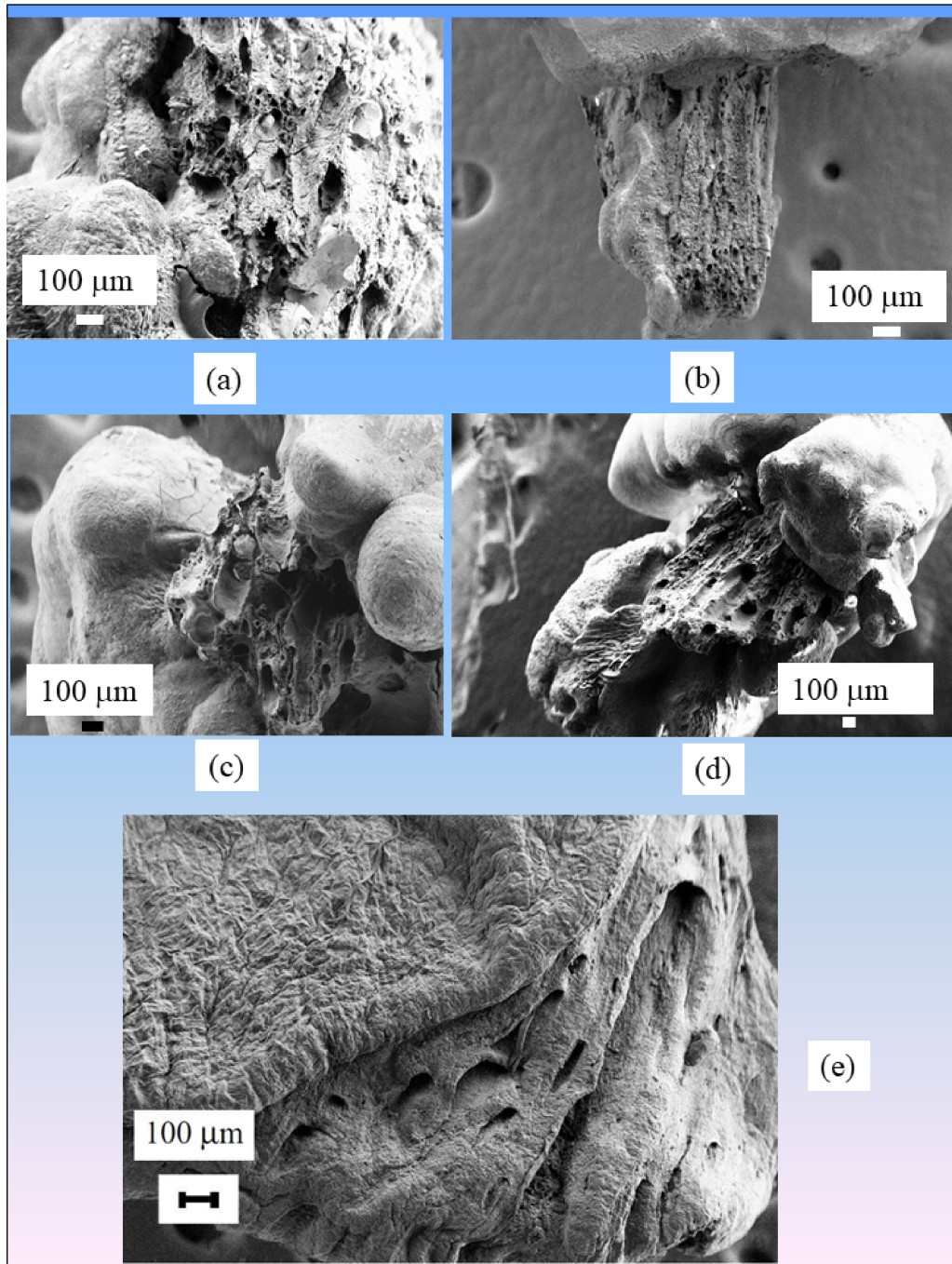


Figure 6. (a–d) SEM observations of RP made of CA. (e) Tip of the papilla with tubule exits labeled with yellow arrows.

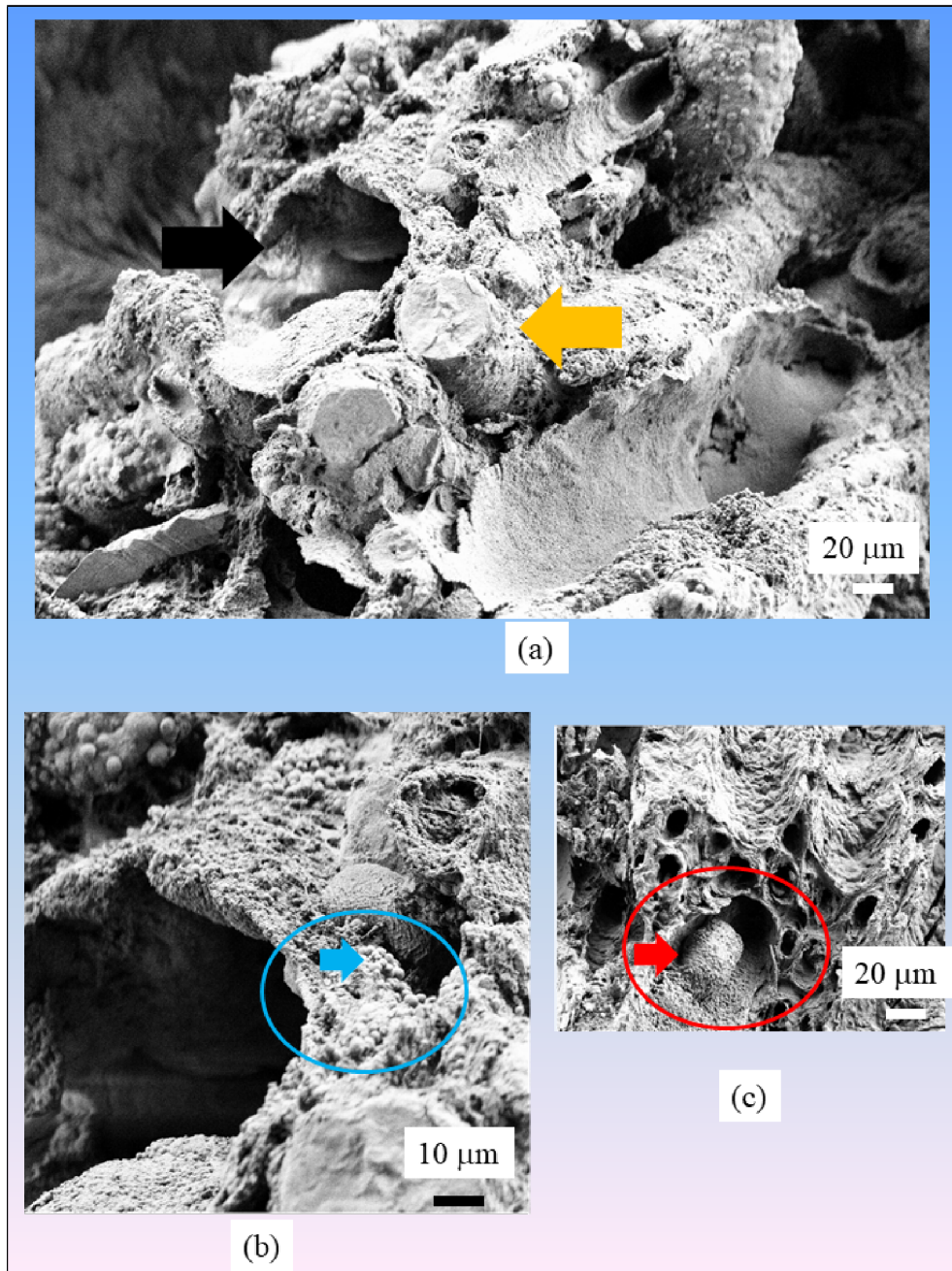


Figure 7. (a–c) SEM observations at high magnification of RP made of CA. (c) Tubular plug in mouse papilla.

face in aqueous conditions. The predictions on the effect of the kinetics on the whewellite morphology is shown in Figure 9, following the discussion reported in Ref. [70].

However, what is striking is the sintered aspect of the (12-1) and (010) surfaces, which is not seen in aqueous conditions. This might be ascribed to the presence of complexing agents such

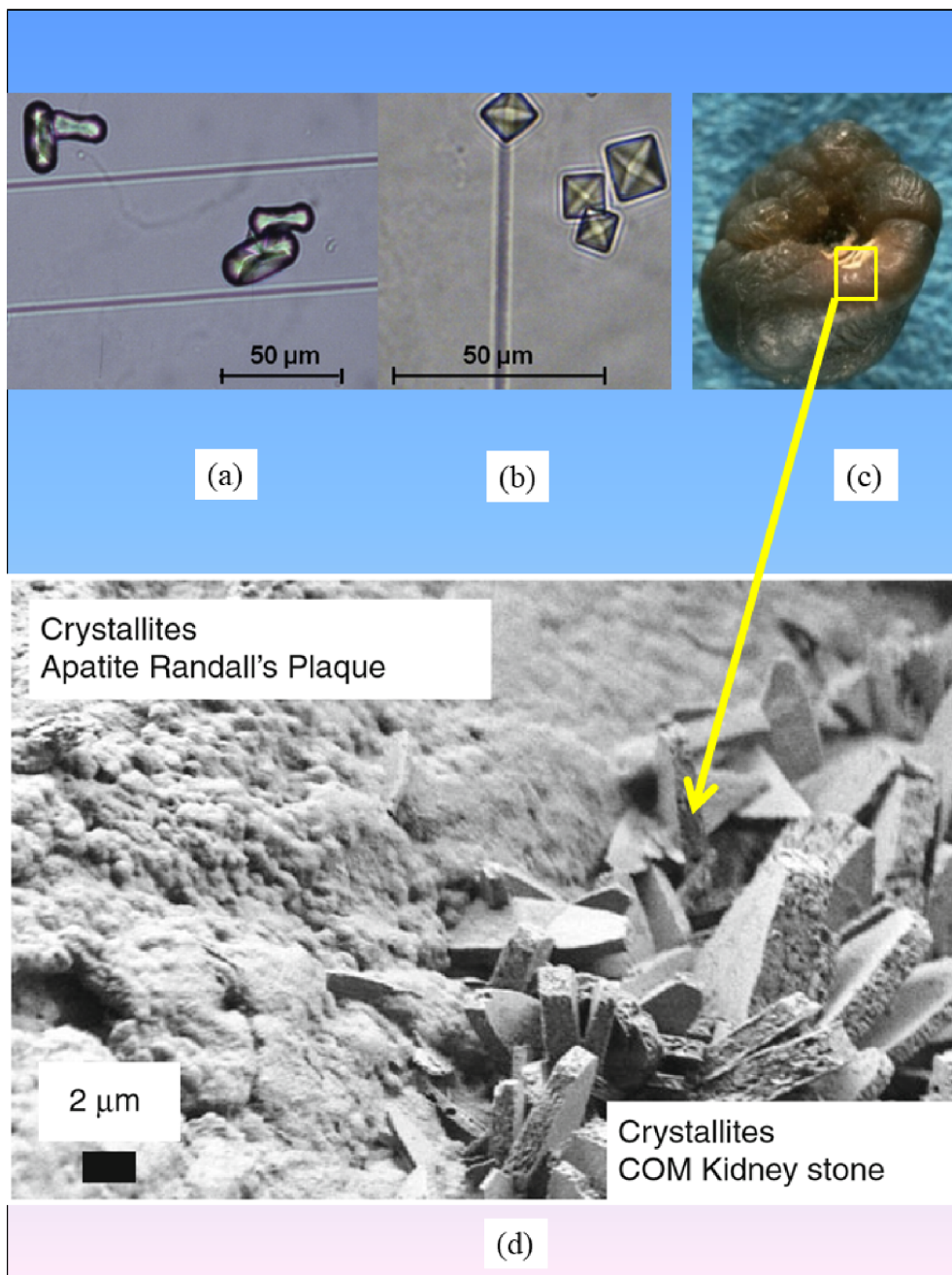


Figure 8. (a) Whewellite and (b) weddellite crystallites in urine. (c) Whewellite KS with RP, yellow square labels the interface between KS and RP. (d) SEM observations of the interface between RP and whewellite KS.

as citrate ion, which is known to modify the kinetics of weddellite polyhydrate nucleation and crystal growth. The sintering also exerts a rela-

tively high impact on surface degradation, which parallels the catechin chelation effect on weddellite [70].

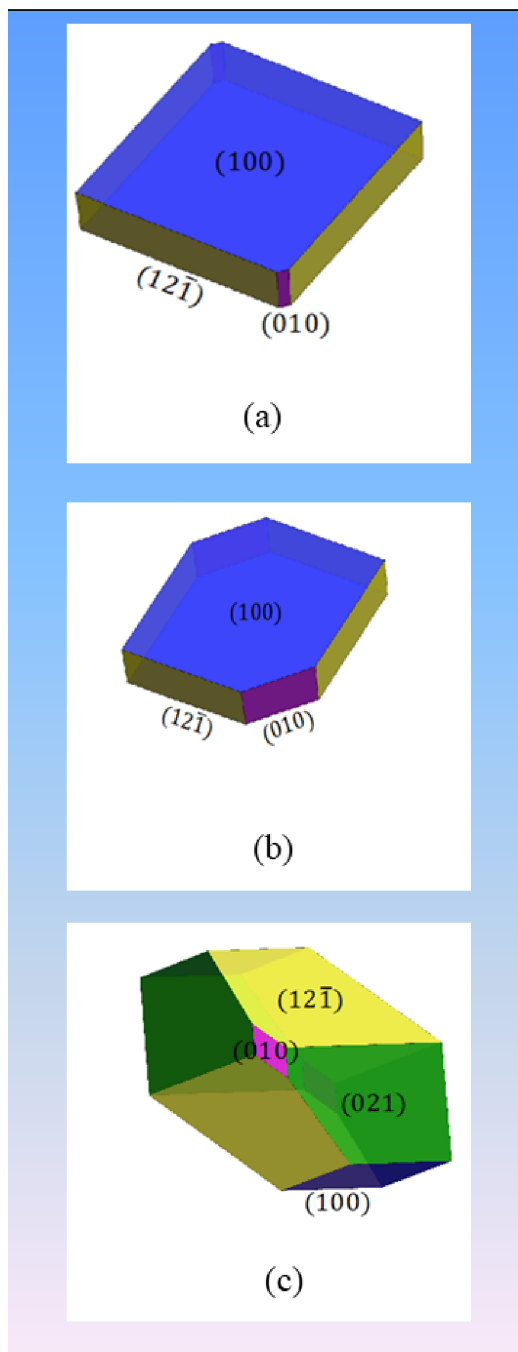


Figure 9. (a) Morphology prediction of COM crystal with the water molecules, without (001) face. (b) Same but with a surface energy correction of $-0.1 \text{ J}\cdot\text{m}^{-2}$ on the (010) face. (c) Same but with energy corrections: $-0.03 \text{ J}\cdot\text{m}^{-2}$ for (021) and (010) surface energies. (Figure adapted from [58].)

8. Elucidating the effect of drugs on kidney stones

In addition to primary hyperoxaluria, several other genetic abnormalities lead to kidney stone pathogenesis, such as inherited distal renal tubular acidosis leading to the formation of calcium phosphate stones with a specific morphology [109], or adenine phosphoribosyltransferase (APRT) deficiency which results in 2,8-dihydroxyadenine (DHA) crystals [110, 111]. Cystinuria, an autosomal recessive disorder, presents a similar picture, leading to stone formation in kidneys and accounting for 1–2% of all cases of urolithiasis. As underlined by Worcester *et al.* [112], cystinuria occupies a unique position among renal stone diseases due to a high recurrence rate. Also, the formation of cystine stones is frequently associated with progression toward chronic kidney disease and renal failure [113–117].

According to the classification of kidney stones [61–64], two distinctive morphologies named type Va (the most common one related to untreated patients) and type Vb (Figures 10a and b) exist. As we can see in Figure 10b, a diffuse concentric structure exists in the periphery of Vb stones with a core of unorganized agglomerates of cystine crystals. SEM shows large crystals displaying flat surfaces with well-defined corners and edges in Va cystine kidney stones (Figure 10c). When the patient follows a conventional treatment based on urine alkalization, significant erosion of the cystine crystal surface occurs (Figure 10d).

Among the results of our investigation [115], it is worth emphasizing that the surface state of cystine crystallites depends on the drug taken by the patient. In a patient treated with tiopronine (Figure 10e), we observed hexagonal holes which correspond to dissolved small cystine crystals, while large ones have lost their typical hexagonal shape. Such a surface state is very different from that observed in a patient treated with captopril (Figure 10e) in which numerous scattered holes, similar to wormholes in a stone, are observed.

9. Biopsy imaging

Scanning and transmission mode electron microscopy of biopsies has been performed for several decades [118–122]. In our investigations, we

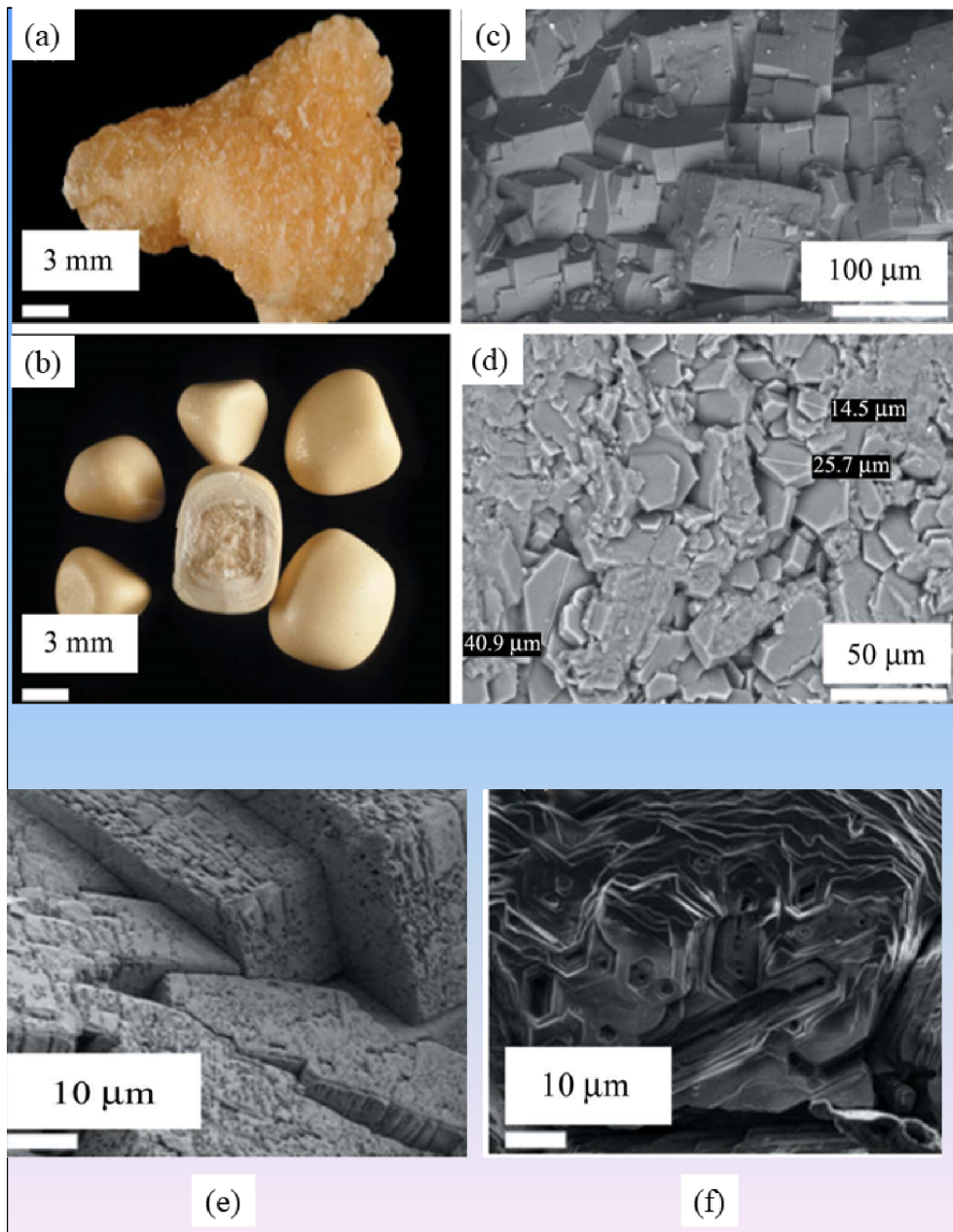


Figure 10. (a) Va cystine kidney stone. (b) Vb cystine kidney stones. (c) SEM image of a typical Va cystine kidney stone. (d) SEM image of a Vb kidney stone. (e) Example of impaired surface of cystine crystals displaying numerous scattered holes similar to wormholes in a stone from a patient treated with captopril. The bulk of the crystals is not affected by such a treatment. (f) Significant erosion of the surface of cystine crystals in a patient treated with tiopronine. Note the hexagonal holes which correspond to dissolved small cystine crystals. Large ones have lost their typical hexagonal shape.

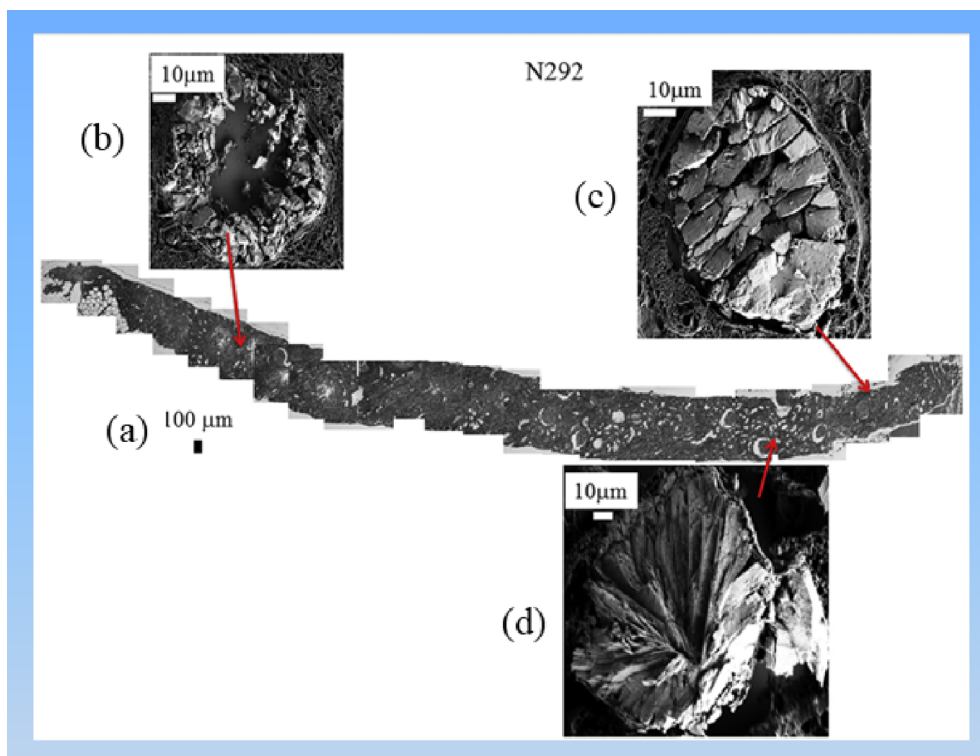


Figure 11. (a) Topology of the different abnormal deposits in kidney biopsy N292. Agglomeration of “large” crystallites is observed in the lumen of tubules (c) while agglomerations of “small” crystallites are located in the tubular cells (b). (d) Radial agglomeration of platelets.

have used FE-SEM on human biopsy tissue coming from various organs namely kidney [123–126], pancreas [127], skin [128–131], hairs [132], breast [26], thyroid [133,134], or arterial wall [135], but of course we must stress that such opportunities exist for cells and mice as well [136–140].

Localization and morphology are two key points which can be addressed through SEM observations on kidney biopsies (Figure 11a). For example, with respect to morphology, small (Figure 11b) and large (Figure 11c) crystallites as well as a radial agglomeration of platelets (Figure 11d) can be observed. Also, it is noteworthy that large crystallites are located in the lumen of tubules (Figure 11c) while “small” ones are in the tubular cells (Figure 11b). It is well known that the composition of the tubule fluid depends on the segment of the nephron. This modulation of the composition along the nephron in addition to various pathological conditions for hyperoxaluria may explain why various configurations can be observed by SEM.

In the case of breast, SEM offers the opportunity to define two different kinds of calcification, namely the well-known plaque easily detected by optical microscopy (Figure 12a), and micrometer and submicrometer spherical entities (Figures 12b and c). Finally, it was possible to relate these two families of calcifications. As we can see in Figure 12d, SEM provides structural evidence that micrometer scale plaques are the result of agglomeration of submicrometer scale spherical calcifications.

Observations at higher magnification underline diversity in the inner structure of the spherical entities (Figure 13), suggesting diversity in the nucleation/growing processes.

Finally, note that not all the spherical structures in tissues are always composed of CA (Figure 14). For instance, in skin calcium carbonate has been detected [128]. It is thus of primary importance to the clinician to precisely identify the chemical composition of spherical entities through either IR or Raman spectroscopies [74,76,141–143].

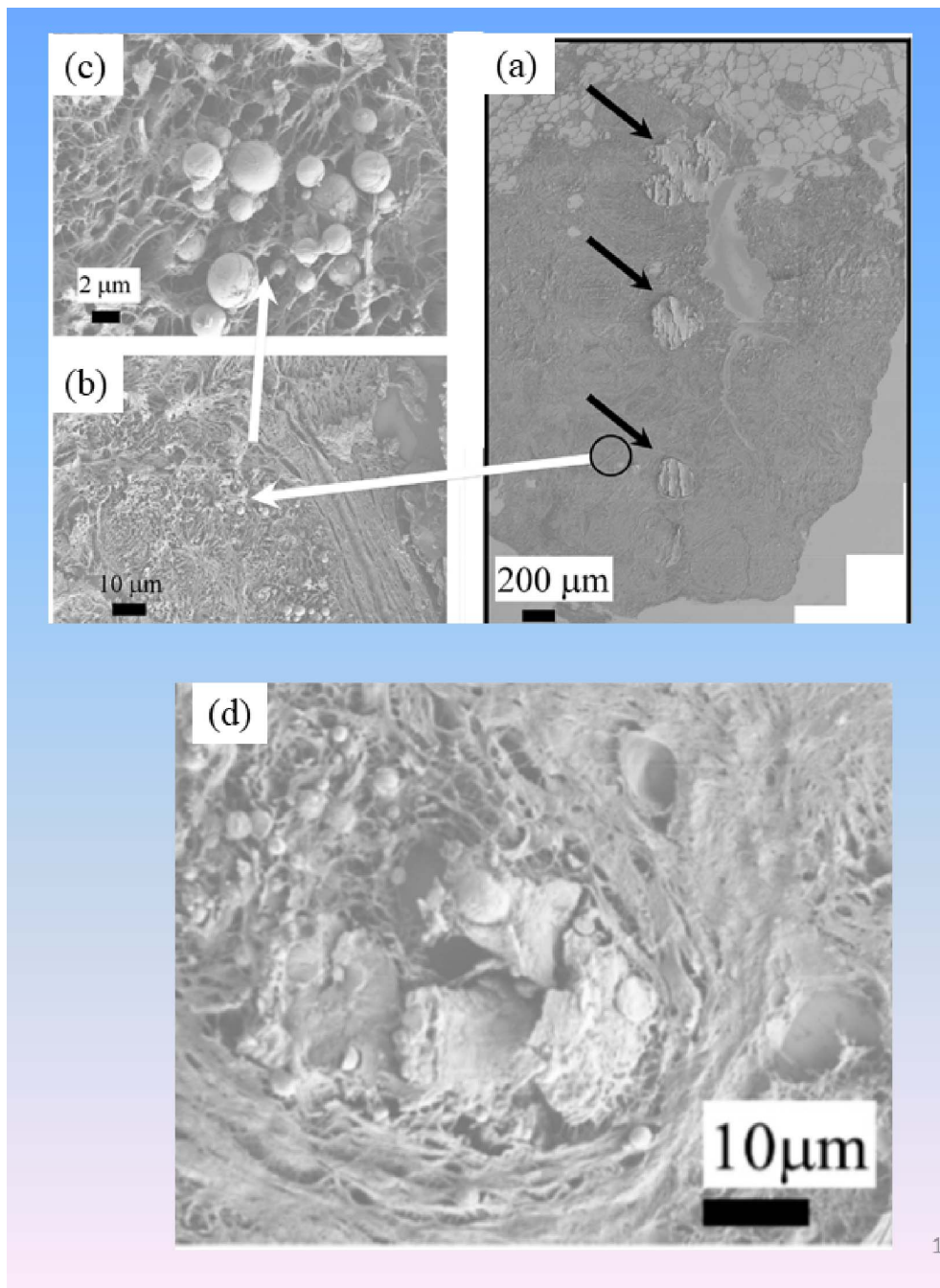


Figure 12. (a) FE-SEM observations of sample 13H2606 (Fibroadenoma) showing heavily mineralized deposits with very small entities invisible at this magnification. (b, c) Submicrometer scale spherules corresponding to the black circle of Figure 2a are visualized at higher magnifications. (d) SEM observations seem to show that “heavily” mineralized deposits are the result of the agglomeration of submicrometer scale spherules.

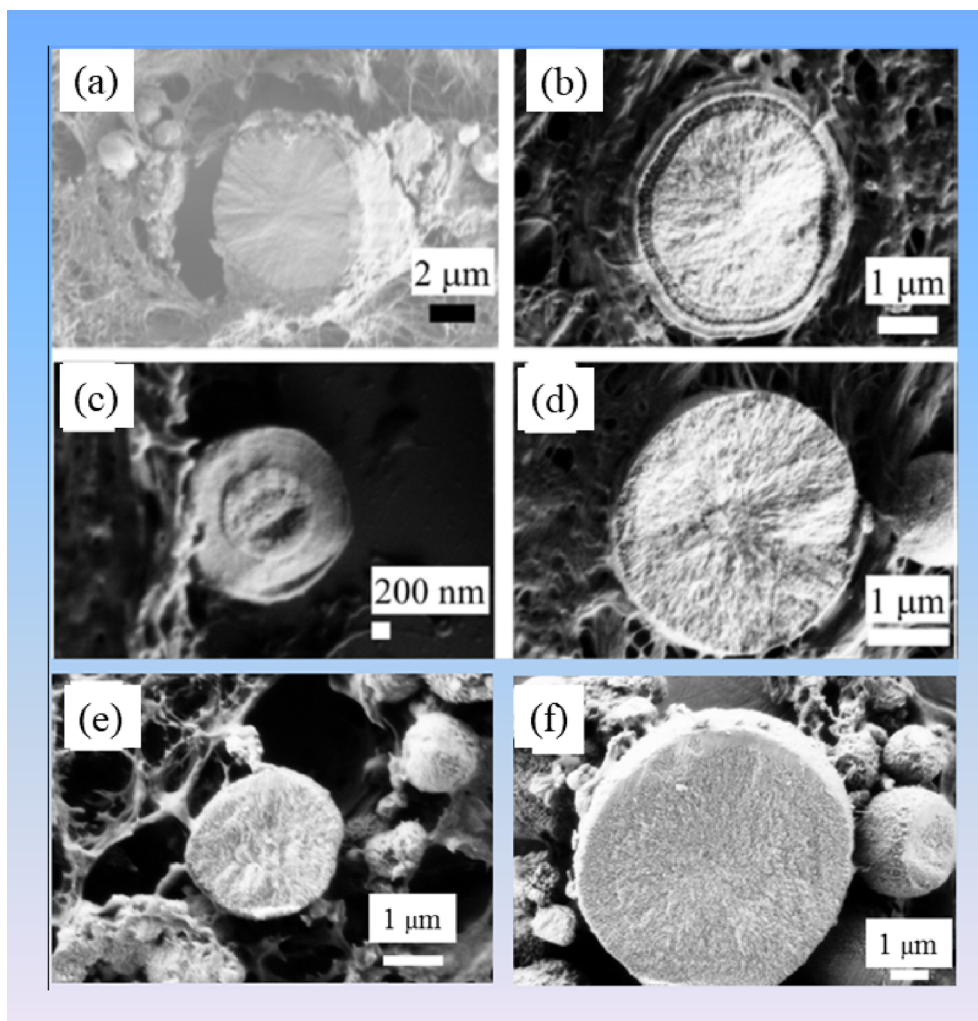


Figure 13. Different internal structures of CA spherulites present in breast (a–d: (a) radial structure; (b, c) concentric layers; (d) radial structure) and kidney (e, f: without structure).

10. Imaging of medical devices

Finally, we must underline that SEM plays an important role in the characterization of the surface of medical devices [39,144–147]. Recently, we have characterized the surface state and the elastic properties of a set of JJ stents [39] on which pathological calcifications were present (Figure 15). It was quite a surprise for the clinicians that black marks on the surface of JJ stents to help urologists during the operation, significantly alter the surface and may ultimately serve as nucleation centers. Note that ureteral replacement devices have also been studied [147].

11. Energy-dispersive X-ray spectroscopy

X-ray fluorescence induced by electron spectroscopy constitutes a powerful technique which allows elemental identification by measuring the number and energy of X-rays emitted from the biological sample after excitation with an electron beam. Even if the detection limit is more important than the one related to X-ray fluorescence induced by protons or photons [148,149], such spectroscopy can give very interesting information regarding the chemistry of pathological calcifications [18,150–153].

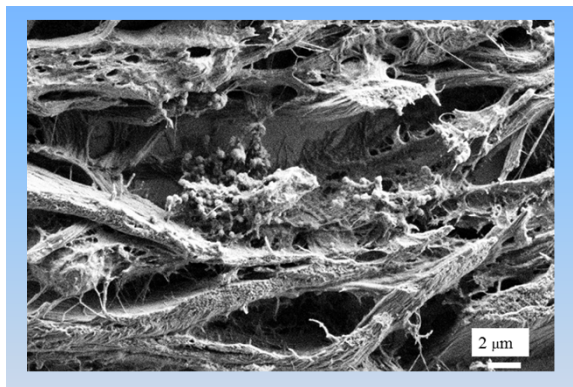


Figure 14. The spheriules present in the skin (for a patient affected by sarcoidosis) are made of calcium carbonate as shown by FTIR spectroscopy and energy dispersive X-ray measurements.

For example, Racek *et al.* [18] have selected a set of 30 samples covering the most common types of human kidney stones for an investigation through SEM coupled with energy-dispersive spectroscopy. After application of standardization, these authors show that it is possible to obtain a quantitative microanalysis with detection limits of 400 ppm (Mg, P, S, Cl, K, Ca), 500 ppm (Na), and 1200 ppm (F). Such spectroscopy can thus bring information regarding the presence of light elements such Mg or F, which are generally not discussed in the case of X-ray fluorescence experiments induced by photons [154–156].

Recently, we have investigated a set of kidney stones containing whitlockite in order to assess the relationship between this chemical compound and infection. Whitlockite is a calcium phosphate phase of crucial interest in several pathologies [157–161]. In order to confirm its presence in kidney stones, we have performed EDX measurements. On Figure 16, SEM observations allow us to underline the presence of pseudocubic crystallites with a trigonal geometry. EDX spectra shows contributions of some of the elements present in the Wk stoichiometric formula $\text{Ca}_9\text{Mg}(\text{HPO}_4)(\text{PO}_4)_6$, namely O, P, Mg, and Ca (Figure 16b).

12. Complementarity with other techniques

In our research dedicated to pathological calcifications, we have tried to take into account the hierar-

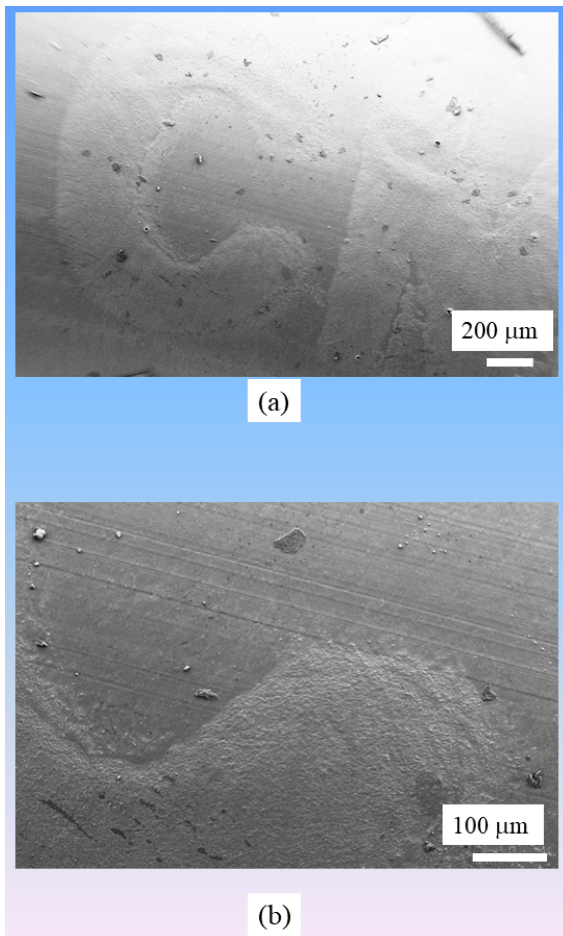


Figure 15. Alteration of the surface state of a JJ stent at black positioning marks.

chical structure as well as the chemical diversity of such biological entities [10,11]. A precise identification of the organic [162] and inorganic parts [163] as well as of the trace elements [148,149] has thus to be performed. To attain this goal, in lab characterization techniques [163–165] as well as ones related to large scale instruments, such synchrotron radiation [166–172] or neutron [72,78,103,166,173,174] facilities are needed.

To describe the hierarchical structure, we have used optical, scanning electron as well as transmission electron (TEM) and scanning transmission electron microscopes (STEM) [89,91,92,175]. We have thus described these biological entities at the millimeter, micrometer, and nanometer scales. If the elementary composition can be given by EDX spec-

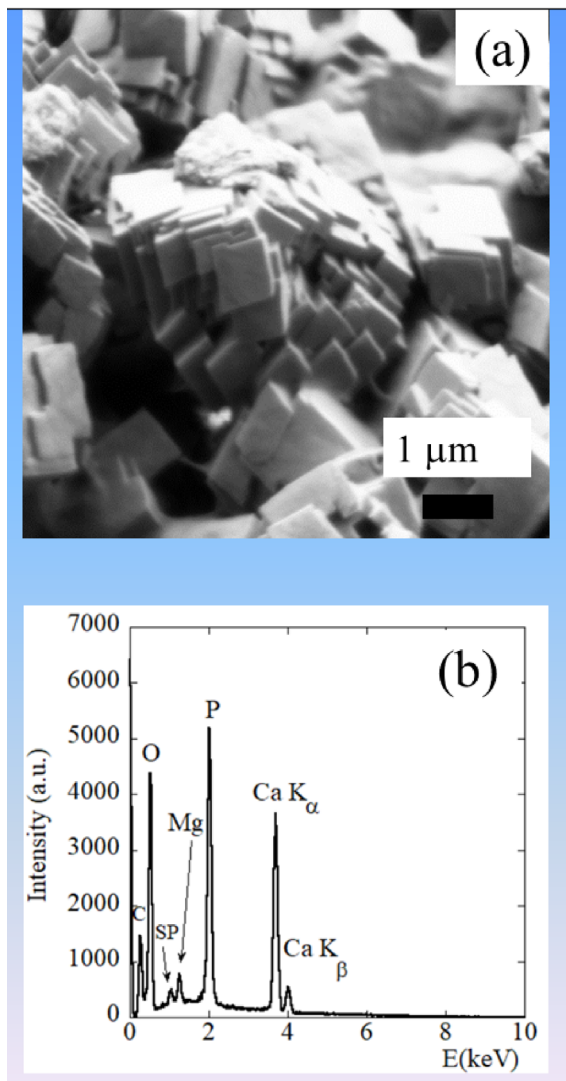


Figure 16. (a) Characteristic pseudocubic morphology of Wk as seen by FE-SEM and corresponding EDX spectrum, (b) in which the contributions of C ($K_{\alpha} = 0.277$ keV), O ($K_{\alpha} = 0.525$ keV), Mg ($K_{\alpha} = 1.253$ keV), P ($K_{\alpha} = 2.014$ keV), and Ca ($K_{\alpha} = 3.691$ keV, $K_{\beta} = 4.012$ keV) are clear. Note the presence of a sum peak (SP) due to the coincidence of two O K_{α} photons.

troscopy at submicrometer scale, other X-ray fluorescence spectroscopy which are more sensitive but associated with less spatial resolution can give complementary information [176,177]. Regarding elec-

tron microscopy, electron energy-loss spectroscopy can be used to describe the local environment of elements and can be thus considered as a very exciting way to complete information given by EDX spectroscopy. Recent studies have proved that EELS can provide highly relevant information concerning the formation mechanisms of these entities [175,178–182].

Finally, X-ray absorption spectroscopy [183–185], which uses synchrotron radiation as a probe, offers major structural and electronic information regarding the local structure of materials of medical interest encompassing those without long range order such as Pt anticancer molecules [123,138,186] or nanometer scale particles [187–190]. In our case, we have used XAS to describe the local environment of trace elements present in different pathological calcifications [155,169,191–193], thus obtaining a more precise chemical description than the one obtained by EDX spectroscopy but quite similar to the ones gathered by EELS [175,178–182].

13. A major perspective: environmental SEM

Among the different major developments related to SEM, we have to underline the one published by Robinson [194,195], which has modified the vacuum system of a scanning electron microscope in order to be able to study hydrated specimens. According to this pioneer work, such modification has enabled the observation of biological specimens partially immersed in water at temperatures just above 0 °C with a spatial resolution of approximately 0.2 μm.

Thanks to several major improvements, environmental SEM now constitutes an indispensable tool for life and medical sciences [196–198]. Environmental SEM offers a unique opportunity to image wet and insulating materials such as bacteria biofilm [199–201]. At this point, it is worth to underline that special attention has to be paid to the protocol preparation in order to avoid effects of irradiation [202,203]. In some publications, the possibility to collect SEM images of live cells as well as live bacteria has been underlined and a recent publication has discussed this possibility [204].

Regarding urology, environmental SEM has been used to investigate the formation of biofilm on medical device [205,206]. Recently, Fernández-Delgado *et al.* [206] have used environment SEM to study the

pathogenesis of biofilm on the surface of urinary catheters induced by a human pathogen namely *Proteus mirabilis*. Their study shows, for the first time, the ability of clinical and environmental *P. mirabilis* strains to develop contrasting biofilms on chitin and stainless steel surfaces. In the case of pathological calcifications, environmental SEM may play an important role for a better understanding of the relationship between bacteria and struvite, for example [207].

14. Conclusion

The selected examples discussed clearly show that SEM constitutes a major tool used in many research fields encompassing medical diagnosis, the action of drugs on concretions (here KS), and the description of growth processes of pathological calcifications. Actually, SEM acts at the interfaces between medical diagnosis and research in addressing challenging issues. However, it is quite probable that SEM devices will soon be introduced into anatomical pathology laboratories. Moreover, combined with other characterization and modeling techniques, we can expect exploration and understanding the origin of calcifications at the atomic scale. This concerted approach will enable us to tackle the multi-scale challenge of linking medical diagnosis with the atomic structure of the pathology.

Acknowledgments

This work was supported by the Physics and Chemistry Institutes of Centre national de la recherche scientifique and by contracts ANR-09-BLAN-0120-02, ANR-12-BS080022, ANR-13-JSV-10010-01, convergence UPMC CVG1205, and CORDDIM-2013-COD130042.

References

- [1] E. Ruska, "The development of the electron microscope and of Electron microscopy (Nobel Lecture)", *Angewandte Chemie International Edition in English*, 1987, **26**, no. 7, 595-605.
- [2] A. Bogner, P. H. Jouneau, G. Thollet, D. Basset, C. Gauthier, *Micron*, 2007, **38**, 390-401.
- [3] F. Brisset, M. Repoux, J. Ruste, F. Grillon, F. Robaut, *Microscopie Electronique à Balayage et Microanalyses*, EDP Sciences, 2009, ISBN: 978-2759823222.
- [4] P. M. Andrews, K. R. Porter, *Am. J. Anat.*, 1974, **140**, 81-116.
- [5] T. Fujita, J. Tokunaga, M. Edanaga, *Cell Tissue Res.*, 1976, **166**, 299-314.
- [6] F. Phaneuf-Mimeault, R. Tawashi, *Eur. Urol.*, 1977, **3**, 171-175.
- [7] S. R. Khan, R. L. Hackett, *J. Urol.*, 1986, **135**, 818-825.
- [8] A. Oren, H. Husdan, P.-T. Cheng, R. Khanna, A. Pierratos, G. Digenis, D. Oreopoulos, *Kidney Int.*, 1984, **25**, 534-538.
- [9] P. T. Cheng, K. P. H. Pritzker, J. Tausch, A. Pittaway, J. Millard, *Scanning Electron Microsc. III*, 1981, **1**, 163-168.
- [10] D. Bazin, M. Daudon, C. Combes, C. Rey, *Chem. Rev.*, 2012, **112**, 5092-5120.
- [11] D. Bazin, M. Daudon, *J. Phys. D: Appl. Phys.*, 2012, **45**, article no. 383001.
- [12] D. Bazin, J.-P. Haymann, E. Letavernier, J. Rode, M. Daudon, *La Presse médicale*, 2014, **43**, 135-148.
- [13] H. H. Chang, C. L. Cheng, P. J. Huang, S. Y. Lin, *Anal. Bioanal. Chem.*, 2014, **406**, 359-366.
- [14] A. Lionet, M. Haeck, A. Garstka, V. Gnemmi, D. Bazin, E. Letavernier, J.-P. Haymann, C. Noel, M. Daudon, *C. R. Chim.*, 2016, **19**, 1542-1547.
- [15] S. Pramanik, S. Ghosh, A. Roy, R. Mukherjee, A. K. Mukherjee, *Z. Kristallogr. Cryst. Mater.*, 2016, **231**, 97-105.
- [16] A. Dessombz, G. Coulibaly, B. Kirakoya, R. W. Ouedraogo, A. Lengani, S. Rouzière, R. Weil, L. Picaut, C. Bonhomme, F. Babonneau, D. Bazin, M. Daudon, *C. R. Chim.*, 2016, **19**, 1573-1579.
- [17] P. Chatterjee, A. Paramita, A. K. Chakraborty, *Spectrochim. Acta Part A*, 2018, **200**, 33-42.
- [18] M. Racek, J. Racek, I. Hupáková, *Scand. J. Clin. Lab. Invest.*, 2019, **79**, 208-217.
- [19] M. A. P. Manzoor, M. Mujeeburrahiman, P.-D. Rekha, *Urolithiasis*, 2019, **47**, 137-148.
- [20] E. X. Keller, V. de Coninck, M. Audouin, S. Doizi, D. Bazin, M. Daudon, O. Traxer, *J. Biophotonics*, 2019, **12**, article no. e201800227.
- [21] M. G. Baron, N. Benmoussa, D. Bazin, I. Abadie, M. Daudon, P. Charlier, *Urolithiasis*, 2019, **47**, 487-488.
- [22] M. Mirkovića, A. Dosen, S. Erić, P. Vulić, B. Matovića, A. Rosić, *Microchem. J.*, 2020, **152**, article no. 104429.
- [23] J. Zaworski, E. Boudierlique, D. Anglicheau, J.-P. Duong Van Huyen, V. Gnemmi, J.-B. Gibier, Y. Neugebauer, J.-P. Haymann, D. Bazin, V. Frochot, M. Daudon, E. Letavernier, *Kidney Int. Rep.*, 2020, **5**, 737-741.
- [24] V. Frochot, V. Castiglione, I. Lucas, J.-P. Haymann, E. Letavernier, D. Bazin, G. Fogazzi, M. Daudon, *Clin. Chim. Acta*, 2020, **515**, 1-4.
- [25] P. Nolasco, P. V. Coelho, C. Coelho, D. F. Angelo, J. R. Dias, N. M. Alves, A. Maurício, M. F. C. Pereira, A. P. Alves de Matos, R. C. Martins, P. A. Carvalho, *Microsc. Microanal.*, 2019, **25**, 151-163.
- [26] A. Ben Lakhdar, M. Daudon, M. C. Matthieu, A. Kellum, C. Balleyguier, D. Bazin, *C. R. Chim.*, 2016, **19**, 1610-1624.
- [27] R. Scott, C. Kendall, N. Stone, K. Rogers, *Sci. Rep.*, 2017, **7**, article no. 136.
- [28] J. A. M. R. Kunitake, S. Choi, K. X. Nguyen, M. M. Lee, F. He, D. Sudilovsky, P. G. Morris, M. S. Jochelson, C. A. Hudis, D. A. Muller, P. Fratzl, C. Fischbach, A. Masic, L. A. Estroff, *J. Struct. Biol.*, 2018, **202**, 25-34.

- [29] S. C. Curtze, M. Kratz, M. Steinert, S. Vogta, *Sci. Rep.*, 2016, **6**, article no. 23285.
- [30] P. Dorfmueller, D. Bazin, S. Aubert, R. Weil, F. Brisset, M. Daudon, F. Capron, I. Brochériou, *Cardiol. Res. Pract.*, 2010, article no. 685926.
- [31] C. Nguyen, D. Bazin, M. Daudon, A. Chatron-Colliet, D. Hannonouche, A. Bianchi, D. Côme, A. So, N. Busso, F. Lioté, H.-K. Ea, *Arthritis Res. Ther.*, 2013, **15**, article no. R103.
- [32] H.-K. Ea, C. Nguyen, D. Bazin, A. Bianchi, J. Guicheux, P. Reboul, M. Daudon, F. Lioté, *Arthritis Rheum.*, 2010, **63**, 10-18.
- [33] H. A. Almarshad, S. M. Badawy, A. F. Alsharari, *Comb. Chem. High Throughput Screen.*, 2018, **21**, 495-500.
- [34] A. Dessombz, P. Méria, D. Bazin, M. Daudon, *PLoS One*, 2012, **7**, article no. e51691.
- [35] A. Dessombz, P. Méria, D. Bazin, E. Foy, S. Rouzière, R. Weil, M. Daudon, *Prog. Urol.*, 2011, **21**, 940-945.
- [36] S. De Santis, G. Sotgiu, A. Crescenzi, C. Taffon, A. Felici, M. Orsini, *J. Pharm. Biomed. Anal.*, 2020, **190**, article no. 113534.
- [37] M. Olaya, S. Aldana, M. Maya, F. Gil, *J. Dev. Orig. Health Dis.*, 2017, **8**, 613-617.
- [38] A.-L. Faucon, M. Daudon, V. Frochot, D. Bazin, B. Terris, V. Caudwell, *Kidney Int.*, 2018, **93**, 1251-1252.
- [39] C. Poulard, A. Dessombz, M. Daudon, D. Bazin, *C. R. Chim.*, 2016, **19**, 1597-1604.
- [40] D. Bazin, M. Daudon, *Ann. Biol. Clin.*, 2015, **73**, 517-534.
- [41] M. Daudon, P. Jungers, D. Bazin, *N. Engl. J. Med.*, 2008, **359**, 100-102.
- [42] M. Daudon, P. Jungers, D. Bazin, *N. Engl. J. Med.*, 2009, **360**, 1680.
- [43] H. Miyazaki, H. Uozaki, A. Tojo, S. Hirashima, S. Inaga, K. Sakuma, Y. Morishita, M. Fukayama, *Pathol. Res. Pract.*, 2012, **208**, 503-509.
- [44] C. Dittmayer, E. Wolcker, I. Wacker, R. R. Schröder, S. Bachmann, *Kidney Int.*, 2018, **94**, 625-631.
- [45] D. Bazin, C. Jouanneau, S. Bertazzo, C. Sandt, A. Dessombz, M. Réfrégiers, P. Dumas, J. Frederick, J.-P. Haymann, E. Letavernier, P. Ronco, M. Daudon, *C. R. Chim.*, 2016, **19**, 1439-1450.
- [46] E. Esteve, C. Jouanneau, E. Letavernier, P. Ronco, M. Daudon, D. Bazin, M. Réfrégiers, *Nephrol. Ther.*, 2015, **11**, 279.
- [47] D. Bazin, E. Letavernier, J. P. Haymann, V. Frochot, M. Daudon, *Ann. Biol. Clin.*, 2020, **78**, 349-362.
- [48] N. Vidavsky, J. A. M. R. Kunitake, L. A. Estroff, *Adv. Healthc. Mater.*, 2020, article no. e2001271.
- [49] M. Van Meerssche, J. Feneau-Dupont, *Introduction à la Cristallographie et à la Chimie Structurale*, Vander, Louvain, 1973.
- [50] T. Kogure, *Dev. Clay Sci.*, 2013, **5**, 275-317.
- [51] R. F. Egerton, *Physical Principles of Electron Microscopy: An Introduction to TEM, SEM, and AEM*, Springer, New York, 2005, 202 pages.
- [52] B. J. Griffin, *Scanning*, 2011, **33**, 162-173.
- [53] D. A. Moncrieff, P. R. Barker, *Scanning*, 1978, **1**, 195-197.
- [54] D. C. Joy, *Ultramicroscopy*, 1991, **37**, 216-233.
- [55] K. de Haan, Z. S. Ballard, Y. Rivenson, Y. Wu, A. Ozcan, *Sci. Rep.*, 2019, **9**, article no. 12050.
- [56] A. E. Vladár, M. T. Postek, B. Ming, *Microsc. Today*, 2009, **17**, 6-13.
- [57] D. C. Joy, *AIP Conf. Proc.*, 2005, **788**, 535-542.
- [58] S. P. Collins, R. K. Pope, R. W. Scheetz, R. I. Ray, P. A. Wagner, B. J. Little, *Microsc. Res. Tech.*, 1993, **25**, 398-405.
- [59] S. E. Kirk, J. N. Skepper, A. M. Donald, *J. Microsc.*, 2009, **233**, 205-224.
- [60] D. B. Peckys, J.-P. Baudoin, M. Eder, U. Werner, N. de Jonge, *Sci. Rep.*, 2013, **3**, article no. 2626.
- [61] M. Daudon, C. A. Bader, P. Jungers, *Scanning Microsc.*, 1993, **7**, 1081-1104.
- [62] M. Daudon, *Ann. Urol.*, 2005, **39**, 209-231.
- [63] M. Daudon, P. Jungers, "Stone composition and morphology: a window on etiology", in *Urolithiasis: Basic Science and Clinical Practice* (J. J. Talati, H. G. Tiselius, D. M. Albalá, Z. Ye, eds.), Springer, London, 2012, 113-140.
- [64] M. Daudon, A. Dessombz, V. Frochot, E. Letavernier, J.-P. Haymann, P. Jungers, D. Bazin, *C. R. Chim.*, 2016, **19**, 1470-1491.
- [65] J. N. Lalena, *Crystallogr. Rev.*, 2006, **12**, 125-180.
- [66] H. Kubbinga, *Z. Kristallogr.*, 2012, **227**, 1-26.
- [67] G. Wulff, *Z. Kristallogr.*, 1901, **34**, 449-530.
- [68] Y. Zhang, *Trop. J. Pharm. Res.*, 2014, **13**, 829-834.
- [69] J. C. Givand, R. W. Rousseau, P. J. Ludovice, *J. Cryst. Growth*, 1998, **194**, 228-238.
- [70] T. Debroise, T. Sedzik, J. Vekeman, Y. Su, C. Bonhomme, F. Tielens, *Cryst. Growth Des.*, 2020, **20**, 3807-3815.
- [71] I. Petit, G. D. Belletti, T. Debroise, M. Llansola, I. T. Lucas, C. Leroy, C. Bonhomme, L. Bonhomme-Coury, D. Bazin, M. Daudon, E. Letavernier, J. P. Haymann, V. Frochot, F. Babonneau, P. Quaino, F. Tielens, *ChemistrySelect*, 2018, **3**, 8801-8812.
- [72] M. Daudon, D. Bazin, G. André, P. Jungers, A. Cousson, P. Chevallier, E. Véron, G. Matzen, *J. Appl. Cryst.*, 2009, **42**, 109-115.
- [73] X. Carpentier, M. Daudon, O. Traxer, P. Jungers, A. Mazouyes, G. Matzen, E. Véron, D. Bazin, *Urology*, 2009, **73**, 968-975.
- [74] L. Estepa, M. Daudon, *Biospectroscopy*, 1997, **3**, 347-369.
- [75] M. L. Giannossi, *J. X-Ray Sci. Technol.*, 2015, **23**, 401-407.
- [76] M. Daudon, D. Bazin, *C. R. Chim.*, 2016, **19**, 1416-1423.
- [77] M. Daudon, V. Frochot, D. Bazin, P. Jungers, *C. R. Chim.*, 2016, **19**, 1514-1526.
- [78] D. Bazin, G. André, R. Weil, G. Matzen, E. Véron, X. Carpentier, M. Daudon, *Urology*, 2012, **79**, 786-790.
- [79] W. Lopes, G. N. F. Cruz, M. L. Rodrigues, M. H. Vainstein, L. Kmetzsch, C. C. Staats, M. H. Vainstein, A. Schrank, *Sci. Rep.*, 2020, **10**, article no. 2362.
- [80] A. Randall, *N. Engl. J. Med.*, 1936, **214**, 234-237.
- [81] A. Randall, *Ann. Surg.*, 1937, **105**, 1009-1027.
- [82] A. P. Evan, J. E. Lingeman, F. L. Coe, J. H. Parks, S. B. Bledsoe, Y. Shao, A. J. Sommer, R. F. Paterson, R. L. Kuo, M. Grynepas, *J. Clin. Invest.*, 2003, **111**, 607-616.
- [83] M. Daudon, O. Traxer, P. Jungers, D. Bazin, *AIP Conf. Proc.*, 2007, **900**, 26-34.
- [84] X. Carpentier, D. Bazin, P. Jungers, S. Reguer, D. Thiaudière, M. Daudon, *J. Synchrotron Radiat.*, 2010, **17**, 374-379.
- [85] M. Daudon, P. Jungers, D. Bazin, *AIP Conf. Proc.*, 2008, **1049**, 199-215.
- [86] X. Carpentier, D. Bazin, C. Combes, A. Mazouyes, S. Rouzière, P.-A. Albouy, E. Foy, M. Daudon, *J. Trace Elem. Med. Biol.*, 2011, **25**, 160-165.

- [87] M. Daudon, D. Bazin, E. Letavernier, *Urolithiasis*, 2015, **43**, 5-11.
- [88] E. Letavernier, D. Bazin, M. Daudon, *C. R. Chim.*, 2016, **19**, 1456-1460.
- [89] C. Verrier, D. Bazin, L. Huguet, O. Stéphan, A. Gloter, M.-C. Verpont, V. Frochot, J.-P. Haymann, I. Brocheriou, O. Traxer, M. Daudon, E. Letavernier, *J. Urol.*, 2016, **196**, 1566-1574.
- [90] D. Bazin, E. Letavernier, C. Jouanneau, P. Ronco, C. Sandt, P. Dumas, G. Matzen, E. Véron, J.-P. Haymann, O. Traxe, P. Conort, M. Daudon, *C. R. Chim.*, 2016, **19**, 1461-1469.
- [91] E. Letavernier, G. Kauffenstein, L. Huguet, N. Navasiolava, E. Boudierlique, E. Tang, L. Delaitre, D. Bazin, M. de Frutos, C. Gay, J. Perez, M. C. Verpont, J.-P. Haymann, V. Pomozi, J. Zoll, O. Le Saux, M. Daudon, G. Leftheriotis, L. Martin, *J. Am. Soc. Nephrol.*, 2018, **29**, 2337-2347.
- [92] E. Boudierlique, E. Tang, J. Perez, A. Coudert, D. Bazin, M.-C. Verpont, C. Duranton, I. Rubera, J.-P. Haymann, G. Leftheriotis, L. Martin, M. Daudon, E. Letavernier, *Am. J. Pathol.*, 2019, **189**, 2171-2180.
- [93] M. Daudon, O. Traxer, J. C. Williams, D. Bazin, "Randall's Plaque", in *Urinary Tract Stone Disease* (N. P. Rao, G. M. Preminger, J. P. Kavangh, eds.), Springer, New York, 2011, ISBN 978-1-84800-361-3.
- [94] I. Sethmann, G. Wendt-Nordahl, T. Knoll, F. Enzmann, L. Simon, H.-J. Kleebe, *Urolithiasis*, 2017, **45**, 235-248.
- [95] N. Çiftçioğlu, K. Vajdani, O. Lee, G. Mathew, K. M. Aho, E. O. Kajander, D. S. McKay, J. A. Jones, M. L. Stoller, *Int. J. Nanomed.*, 2008, **3**, 105-115.
- [96] L. C. Delatte, J. L. R. Minon-Cifuentes, J. A. Medina, *J. Urol.*, 1985, **133**, 490-494.
- [97] E. Pieras, A. Costa-Bauzá, M. Ramis, F. Grases, *Sci. World J.*, 2006, **6**, 2411-2419.
- [98] L. Huguet, M. Le Dudal, M. Livrozet, D. Bazin, V. Frochot, J. Perez, J. P. Haymann, I. Brocheriou, M. Daudon, E. Letavernier, *Urolithiasis*, 2018, **46**, 333-341.
- [99] A. P. Evan, F. L. Coe, J. E. Lingeman, Y. Shao, A. J. Sommer, S. B. Bledsoe, J. C. Anderson, E. M. Worcester, *Anat. Rec.*, 2007, **290**, 1315-1323.
- [100] S. R. Khan, B. K. Canales, *Urolithiasis*, 2015, **43**, 109-123.
- [101] H. V. Nguyen, M. Daudon, R. J. Réveillaud, P. Jungers, *Nephrologie*, 1987, **8**, 65-69.
- [102] D. Eichert, C. Combes, C. Drouet, C. Rey, *Key Eng. Mater.*, 2005, **284-286**, 3-6.
- [103] D. Bazin, C. Chappard, C. Combes, X. Carpentier, S. Rouzière, G. André, G. Matzen, M. Allix, D. Thiaudière, S. Reguer, P. Jungers, M. Daudon, *Osteoporos. Int.*, 2009, **20**, 1065-1075.
- [104] C. Rey, C. Combes, C. Drouet, S. Cazalbou, D. Grossin, F. Brouillet, S. Sarda, *Progress in Crystal Growth and Characterization of Materials*, vol. 60, Elsevier, 2014, 63-73 pages.
- [105] A. Millan, *Cryst. Growth Des.*, 2001, **1**, 245-254.
- [106] D. Bazin, F. Tielens, *Appl. Catal.*, 2015, **504**, 631-641.
- [107] F. Tielens, D. Bazin, *C. R. Chim.*, 2018, **21**, 174-181.
- [108] I. C. Oguz, H. Guesmi, D. Bazin, F. Tielens, *J. Phys. Chem. C*, 2019, **123**, 20314-20318.
- [109] A. Dessombz, E. Letavernier, J.-P. Haymann, D. Bazin, M. Daudon, *J. Urol.*, 2015, **193**, 1564-1569.
- [110] G. Bollé, C. Dollinger, L. Boutaud, D. Guillemot, A. Bensman, J. Harambat, P. Deteix, M. Daudon, B. Knebelmann, I. Ceballos-Picot, *J. Am. Soc. Nephrol.*, 2010, **21**, 679-688.
- [111] A. Dessombz, D. Bazin, P. Dumas, C. Sandt, J. Sule-Suso, M. Daudon, *PLoS One*, 2011, **6**, article no. e28007.
- [112] E. M. Worcester, J. H. Parks, A. P. Evan, F. L. Coe, *J. Urol.*, 2006, **176**, 600-603.
- [113] E. Letavernier, O. Traxer, J.-P. Haymann, D. Bazin, M. Daudon, *Prog. Urol. - FMC*, 2012, **22**, F119-F123.
- [114] B. Hannache, D. Bazin, A. Boutefnouchet, M. Daudon, *Prog. Urol.*, 2012, **22**, 577-582.
- [115] D. Bazin, M. Daudon, A. Gilles, R. Weil, E. Véron, G. Matzen, *J. Appl. Cryst.*, 2014, **47**, 719-725.
- [116] M. Livrozet, S. Vandermeersch, L. Mesnard, E. Thioulouse, J. Jaubert, J.-J. Boffa, J.-P. Haymann, L. Baud, D. Bazin, M. Daudon, E. Letavernier, *PLoS One*, 2014, **9**, article no. e102700.
- [117] J. P. Haymann, M. Livrozet, J. Rode, S. Doizi, O. Traxer, V. Frochot, E. Letavernier, D. Bazin, M. Daudon, *Prog. Urol. - FMC*, 2021, **31**, F1-F7.
- [118] J. V. Johannessen, *Kidney Int.*, 1973, **3**, 46-50.
- [119] Y. Collan, P. Hirsimäki, H. Aho, M. Wuorela, J. Sundström, R. Terti, K. Metsärinne, *Ultrastruct. Pathol.*, 2005, **29**, 461-468.
- [120] S. Conti, N. perico, R. Novelli, C. Carra, A. benigni, G. Remuzzi, *Sci. Rep.*, 2018, **8**, article no. 4909.
- [121] W.-L. Ng, K. F. So, P. C. So, H. K. Ngai, *Pathology*, 1982, **14**, 299-302.
- [122] H. Miyazaki, H. Uozakia, A. Tojo, S. Hirashima, S. Inaga, K. Sakuma, Y. Morishita, M. Fukayama, *Path. Res. Pract.*, 2012, **208**, 503-509.
- [123] E. Esteve, D. Bazin, C. Jouanneau, S. Rouzière, A. Bataille, A. Kellum, K. Provost, C. Mocuta, S. Reguer, P. Ronco, J. Rehr, J.-P. Haymann, E. Letavernier, A. Hertig, *C. R. Chim.*, 2016, **19**, 1586-1589.
- [124] D. Bazin, E. Letavernier, J.-P. Haymann, F. Tielens, A. Kellum, M. Daudon, *C. R. Chim.*, 2016, **19**, 1548-1557.
- [125] V. Frochot, D. Bazin, E. Letavernier, C. Jouanneau, J.-P. Haymann, M. Daudon, *C. R. Chim.*, 2016, **19**, 1565-1572.
- [126] M. Daudon, V. Frochot, D. Bazin, P. Jungers, *Drugs*, 2018, **78**, 163-201.
- [127] J. Cros, D. Bazin, A. Kellum, V. Rebours, M. Daudon, *C. R. Chim.*, 2016, **19**, 1642-1655.
- [128] H. Colboc, D. Bazin, P. Moguelet, V. Frochot, R. Weil, E. Letavernier, C. Jouanneau, C. Frances, C. Bachmeyer, J.-F. Bernaudin, M. Daudon, *C. R. Chim.*, 2016, **19**, 1631-1641.
- [129] H. Colboc, P. Moguelet, D. Bazin, C. Bachmeyer, V. Frochot, R. Weil, E. Letavernier, C. Jouanneau, M. Daudon, J. F. Bernaudin, *J. Eur. Acad. Dermatol. Venereol.*, 2019, **33**, 198-203.
- [130] H. Colboc, P. Moguelet, D. Bazin, P. Carvalho, A.-S. Dillies, G. Chaby, H. Maillard, D. Kottler, E. Goujon, C. Jurus, M. Panaye, V. Frochot, E. Letavernier, M. Daudon, I. Lucas, R. Weil, P. Courville, J.-B. Monfort, F. Chasset, P. Senet, *JAMA Dermatol.*, 2019, **155**, 789-796.
- [131] H. Colboc, D. Bazin, P. Moguelet, S. Reguer, R. Amode, C. Jouanneau, I. Lucas, L. Deschamps, V. Descamps, N. Kluger, *J. Eur. Acad. Dermatol. Venereol.*, 2020, **34**, e313-e315.
- [132] F. Brunet-Possenti, L. Deschamps, H. Colboc, A. Somogyi, K. Medjoubi, D. Bazin, V. Descamps, *J. Eur. Acad. Dermatol. Venereol.*, 2018, **32**, e442-e443.

- [133] M. Mathonnet, A. Dessombz, D. Bazin, R. Weil, F. Triponez, M. Pusztaszeri, M. Daudon, *C. R. Chim.*, 2016, **19**, 1672-1678.
- [134] J. Guerlain, S. Perie, M. Lefevre, J. Perez, S. Vandermeersch, C. Jouanneau, L. Huguet, V. Frochot, E. Letavernier, R. Weil, S. Rouzière, D. Bazin, M. Daudon, J. P. Haymann, *PLoS One*, 2019, **14**, article no. e0224138.
- [135] R. Coscas, M. Bensussan, M.-P. Jacob, L. Louedec, Z. Massy, Z. Sadoine, M. Daudon, C. Chaussain, D. Bazin, J.-B. Michel, *Atherosclerosis*, 2017, **259**, 60-67.
- [136] F. Preitner, A. Laverriere, S. Metref, A. Da Costa, C. Roger, S. Rotman, D. Bazin, M. Daudon, C. Sandt, A. Dessombz, B. Thorens, *Am. J. Physiol. Renal Physiol.*, 2013, **305**, F786-F795.
- [137] L. Louvet, D. Bazin, J. Büchel, S. Steppan, J. Passlick-Deetjen, Z. A. Massy, *PLoS One*, 2015, **10**, article no. e0115342.
- [138] E. Esteve, D. Bazin, C. Jouanneau, S. Rouzière, A. Bataille, A. Kellum, K. Provost, C. Mocuta, S. Reguer, P. Ronco, J. Rehr, J.-P. Haymann, E. Letavernier, A. Hertig, *C. R. Chim.*, 2016, **19**, 1580-1585.
- [139] C. Bardet, F. Courson, Y. Wu, M. Khaddam, B. Salmon, S. Ribes, J. Thumfart, P. M. Yamaguti, G. Y. Rochefort, M.-L. Figueres, T. Breiderhoff, A. Garcia Castaño, B. Vallée, D. Le Denmat, B. Baroukh, T. Guilbert, A. Schmitt, J.-M. Massé, D. Bazin, G. Lorenz, M. Morawietz, J. Hou, P. Carvalho-Lobato, M. C. Manzanares, J.-C. Fricain, D. Talmud, R. Demontis, F. Neves, D. Zenaty, A. Berdal, A. Kiesow, M. Petzold, S. Menashi, A. Linglart, A. C. Acevedo, R. Vargas-Poussou, D. Müller, P. Houillier, C. Chaussain, *J. Bone Miner. Res.*, 2016, **31**, 498-513.
- [140] H. Bilbault, J. Perez, L. Huguet, S. Vandermeersch, S. Placier, N. Tabibzadeh, V. Frochot, E. Letavernier, D. Bazin, M. Daudon, J.-P. Haymann, *Sci. Rep.*, 2018, **8**, article no. 16319.
- [141] M. Daudon, M. F. Protat, R. J. Reveillaud, H. Jaeschke-Boyerl, *Kidney Int.*, 1983, **23**, 842-850.
- [142] L. Maurice-Estépa, P. Levillain, B. Lacour, M. Daudon, *Scand. J. Urol. Nephrol.*, 1999, **33**, 299-305.
- [143] V. Castiglione, P.-Y. Sacré, E. Cavalier, P. Hubert, R. Gadisseur, E. Ziemons, *PLoS One*, 2018, **13**, article no. e0201460.
- [144] B. A. Vanderbrink, A. R. Rastinehad, M. C. Ost, A. D. Smith, *J. Endourol.*, 2008, **22**, 905-912.
- [145] W.-J. Fu, Z.-X. Wang, G. Li, F.-Z. Cui, Y. Zhang, X. Zhang, *Biomed. Mater.*, 2012, **7**, article no. 065002.
- [146] C. Torrecilla, J. Fernández-Concha, J. R. Cansino, J. A. Mainez, J. H. Amón, S. Costas, O. Angerri, E. Emiliani, M. A. Arrabal Martín, M. A. Arrabal Polo, A. García, M. C. Reina, J. F. Sánchez, A. Budía, D. Pérez-Fentes, F. Grases, A. Costa-Bauzá, J. Cuñé, *BMC Urol.*, 2020, **20**, article no. 65.
- [147] A. Nouaille, A. Descazeaud, F. Desgrandchamps, D. Bazin, M. Daudon, A. Masson Lecomte, P. Mongiat-Artus, P. Méria, *Prog. Urol.*, 2021, **31**, 348-356.
- [148] M. Uo, T. Wada, T. Sugiyama, *Jpn. Dent. Sci. Rev.*, 2015, **51**, 2-9.
- [149] S. Rouzière, D. Bazin, M. Daudon, *C. R. Chim.*, 2016, **19**, 1404-1415.
- [150] V. Uvarov, I. Popov, N. Shapur, T. Abdin, O. N. Gofrit, D. Pode, M. Duvdevani, *Environ. Geochem. Health*, 2011, **33**, 613-622.
- [151] M. S. Yalçın, M. Tek, *J. Appl. Spectrosc.*, 2019, **85**, 1050-1057.
- [152] H. A. Walli, W. J. Abed Ali, *J. Phys.: Conf. Ser.*, 2019, **1294**, article no. 072003.
- [153] K. Seevakan, *Malaya J. Mat.*, 2020, **8**, 1240-1242.
- [154] D. Bazin, P. Chevallier, G. Matzen, P. Jungers, M. Daudon, *Urol. Res.*, 2007, **35**, 179-184.
- [155] A. Dessombz, C. Nguyen, H.-K. Ea, S. Rouzière, E. Foy, D. Hannouche, S. Réguer, F.-E. Picca, D. Thiaudière, F. Lioté, M. Daudon, D. Bazin, *J. Trace Elem. Med. Biol.*, 2013, **27**, 326-333.
- [156] B. Hannache, A. Boutefnouchet, D. Bazin, E. Foy, M. Daudon, *Prog. Urol.*, 2015, **25**, 22-26.
- [157] J. Gervasoni, A. Primiano, P. M. Ferraro, A. Urbani, G. Gambaro, S. Persichilli, *J. Chem.*, 2018, **2018**, article no. 4621256.
- [158] R. Lagier, C. A. Baud, *Pathol. Res. Pract.*, 2003, **199**, 329-335.
- [159] D. Bazin, E. Letavernier, J.-P. Haymann, P. Méria, M. Daudon, *Prog. Urol.*, 2016, **26**, 608-618.
- [160] D. Bazin, M. Daudon, *J. Spect. Imaging*, 2019, **8**, article no. a16.
- [161] D. Bazin, E. Letavernier, J.-P. Haymann, *C. R. Chim.*, 2016, **19**, 1395-1403.
- [162] Y. Li, D. G. Reid, D. Bazin, M. Daudon, M. J. Duer, *C. R. Chim.*, 2016, **19**, 1665-1671.
- [163] M. Daudon, D. Bazin, "New techniques to characterize kidney stones And Randall's plaque", in *Urolithiasis: Basic Science and Clinical Practice* (J. J. Talati, H. G. Tiselius, D. M. Albala, Z. Ye, eds.), Springer, New York, 2012, 683-707.
- [164] H. Colas, L. Bonhomme-Courty, C. Coelho Diogo, F. Tielens, C. Gervais, D. Bazin, D. Laurencin, M. E. Smith, J. V. Hanna, M. Daudon, C. Bonhomme, *Cryst. Eng. Comm.*, 2013, **15**, 8840-8847.
- [165] D. Bazin, C. Leroy, F. Tielens, C. Bonhomme, L. Bonhomme-Courty, F. Damay, D. Le Denmat, J. Sadoine, J. Rode, V. Frochot, E. Letavernier, J.-P. Haymann, M. Daudon, *C. R. Chim.*, 2016, **19**, 1492-1503.
- [166] D. Bazin, M. Daudon, P. Chevallier, S. Rouzière, E. Elkaim, D. Thiaudiere, B. Fayard, E. Foy, P. A. Albouy, G. André, G. Matzen, E. Véron, *Ann. Biol. Clin. (Paris)*, 2006, **64**, 125-139.
- [167] D. Bazin, X. Carpentier, O. Traxer, D. Thiaudière, A. Somygyi, S. Reguer, G. Waychunas, P. Jungers, M. Daudon, *J. Synchrotron Radiat.*, 2008, **15**, 506-509.
- [168] X. Carpentier, D. Bazin, P. Jungers, S. Reguer, D. Thiaudière, M. Daudon, *J. Synchrotron Radiat.*, 2010, **17**, 374-379.
- [169] D. Bazin, M. Daudon, C. Chappard, J. J. Rehr, D. Thiaudière, S. Reguer, *J. Synchrotron Radiat.*, 2011, **18**, 912-918.
- [170] M. Daudon, D. Bazin, *J. Phys.: Conf. Ser.*, 2013, **425**, article no. 022006.
- [171] S. Reguer, C. Mocuta, D. Thiaudière, M. Daudon, D. Bazin, *C. R. Chim.*, 2016, **19**, 1424-1431.
- [172] D. Bazin, M. Daudon, E. Elkaim, A. Le Bail, L. Smrcok, *C. R. Chim.*, 2016, **19**, 1535-1541.
- [173] F. Damay, D. Bazin, M. Daudon, G. André, *C. R. Chim.*, 2016, **19**, 1432-1438.
- [174] M. Daudon, E. Letavernier, R. Weil, E. Véron, G. Matzen, G. André, D. Bazin, *C. R. Chim.*, 2016, **19**, 1527-1534.
- [175] C. Gay, E. Letavernier, M.-C. Verpont, M. Walls, D. Bazin, M. Daudon, N. Nassif, O. Stephan, M. de Fruto, *ACS Nano*, 2020, **14**, 1823-1836.
- [176] E. Esteve, S. Reguer, C. Boissiere, C. Chanéac, G. Lugo,

- C. Jouanneau, C. Mocuta, D. Thiaudière, N. Leclercq, B. Leyh, J. F. Greisch, J. Berthault, M. Daudon, P. Ronco, D. Bazin, *J. Synchrotron Radiat.*, 2017, **24**, 991-999.
- [177] S. Kaščáková, C. M. Kewish, S. Rouzière, F. Schmitt, R. Sobesky, J. Poupon, C. Sandt, B. Francou, A. Somogyi, D. Samuel, E. Jacquemin, A. DubartKupperschmitt, T. H. Nguyen, D. Bazin, J.-C. DuclosVallée, C. Guettier, F. Le Naour, *J. Pathol. Clin. Res.*, 2016, **2**, 175-186.
- [178] M. M. Kłosowski, R. J. Friederichs, R. Nichol, N. Antolin, R. Carzaniga, W. Windl, S. M. Best, S. J. Shefelbine, D. W. McComb, A. E. Porter, *Acta Biomater.*, 2015, **20**, 129-139.
- [179] K. Nitiputri, Q. M. Ramasse, H. Autefage, C. M. McGilvery, S. Boonrungsiman, N. D. Evans, M. M. Stevens, A. E. Porter, *ACS Nano*, 2016, **10**, 6826-6835.
- [180] S. Boonrungsiman, E. Gentleman, R. Carzaniga, N. D. Evans, D. W. McComb, A. E. Porter, M. M. Stevens, *Proc. Natl. Acad. Sci. USA*, 2012, **109**, 14170-14175.
- [181] V. Srot, B. Bussmann, U. Salzberger, J. Deuschle, M. Watanabe, B. Pokorny, I. Jelenko Turinek, A. F. Mark, P. A. van Aken, *ACS Nano*, 2017, **11**, 239-248.
- [182] V. Srot, U. G. K. Wegst, U. Salzberger, C. T. Koch, K. Hahn, P. Kopold, P. A. van Aken, *Micron*, 2013, **48**, 54-64.
- [183] D. E. Sayers, E. A. Stern, F. W. Lytle, *Phys. Rev. Lett.*, 1971, **27**, 1204-1207.
- [184] F. W. Lytle, D. A. Sayers, E. A. Stern, *Phys. Rev. B*, 1975, **11**, 4825-4835.
- [185] E. A. Stern, D. E. Sayers, F. W. Lytle, *Phys. Rev. B*, 1975, **11**, 4836-4846.
- [186] R. Oun, Y. E. Moussa, N. J. Wheate, *Dalton Trans.*, 2018, **47**, 6645-6653.
- [187] X. Yang, M. Yang, B. Pang, M. Vara, Y. Xia, *Chem. Rev.*, 2015, **115**, 10410-10488.
- [188] D. Bazin, D. A. Sayers, J. J. Rehr, *J. Phys. Chem. B*, 1997, **101**, 11040-11050.
- [189] D. Bazin, D. A. Sayers, J. J. Rehr, C. Mottet, *J. Phys. Chem. B*, 1997, **101**, 5332-5336.
- [190] D. Bazin, J. J. Rehr, *J. Phys. Chem. B*, 2003, **107**, 12398-12402.
- [191] D. Bazin, A. Dessombz, C. Nguyen, H. K. Ea, F. Lioté, J. Rehr, C. Chappard, S. Rouzière, D. Thiaudière, S. Reguer, M. Daudon, *J. Synchrotron Radiat.*, 2014, **21**, 136-142.
- [192] C. Nguyen, H. K. Ea, D. Thiaudière, S. Reguer, D. Hannouche, M. Daudon, F. Lioté, D. Bazin, *J. Synchrotron Radiat.*, 2011, **18**, 475-480.
- [193] D. Bazin, X. Carpentier, I. Brocheriou, P. Dorfmueller, S. Aubert, C. Chappard, D. Thiaudière, S. Reguer, G. Waychunas, P. Jungers, M. Daudon, *Biochimie*, 2009, **91**, 1294-1300.
- [194] V. N. Robinson, *J. Microsc.*, 1975, **103**, 71-77.
- [195] V. N. Robinson, *Microsc. Today*, 1997, **5**, 14-15.
- [196] P. Mestres, N. Putz, M. Laue, *Microsc. Microanal.*, 2003, **9**, 490-491.
- [197] S. Thiberge, A. Nechushtan, D. Sprinzak, O. Gileadi, V. Behar, O. Zik, Y. Chowers, S. Michael, J. Schlessinger, E. Moses, *Proc. Natl. Acad. Sci. USA*, 2004, **101**, 3346-3351.
- [198] S. Guthrie, "Exploration of the use of ESEM for the study of biological materials", PhD Thesis, University of Cambridge, UK, 2008.
- [199] I. B. Beech, C. W. S. Cheung, D. B. Johnson, J. R. Smith, *Biofouling*, 1996, **10**, 65-77.
- [200] J. H. Priestler, A. M. Horst, L. C. Van De Werfhorst, J. L. Saleta, L. A. K. Mertes, P. A. Holden, *J. Microbiol. Methods*, 2007, **68**, 577-587.
- [201] L. Bergmans, P. Moisiadis, B. Van Meerbeek, M. Quirynen, P. Lambrechts, *Int. Endod. J.*, 2005, **38**, 775-788.
- [202] A. M. Donald, *Nat. Mater.*, 2003, **2**, 511-516.
- [203] J. E. McGregor, L. T. L. Staniewicz, S. E. Guthrie Neé Kirk, A. M. Donald, *Methods Mol. Biol.*, 2013, **931**, 493-516.
- [204] N. de Jonge, D. B. Peckys, *ACS Nano*, 2016, **10**, 9061-9063.
- [205] A. Trinidad, A. Ibáñez, D. Gómez, J. R. García-Berrocal, R. Ramírez-Camacho, "Application of environmental scanning electron microscopy for study of biofilms in medical devices", in *Microscopy: Science, Technology, Applications and Education* (A. Méndez-Vilas, J. Díaz, eds.), Microscopy Book Series, Formatex Research Center, Badajoz, Spain, 2010, 204-210.
- [206] M. Fernández-Delgado, Z. Duque, H. Rojas, P. Suárez, M. Contreras, M. A. García-Amado, C. Alciaturi, *Ann. Microbiol.*, 2015, **65**, 1401-1409.
- [207] E. J. Espinosa-Ortiz, B. H. Eisner, D. Lange, R. Gerlach, *Nat. Rev. Urol.*, 2019, **16**, 35-53.